LUND UNIVERSITY

Detailed Numerical Simulations of Turbulent Premixed Flames at Moderate and High Karlovitz Numbers

Carlsson, Henning

2014

Link to publication

Citation for published version (APA):
Carlsson, H. (2014). *Detailed Numerical Simulations of Turbulent Premixed Flames at Moderate and High Karlovitz Numbers*. [Doctoral Thesis (compilation), Fluid Mechanics].

Total number of authors:
1

General rights
Unless other specific re-use rights are stated the following general rights apply:
Copyright and moral rights for the publications made accessible in the public portal are retained by the authors and/or other copyright owners and it is a condition of accessing publications that users recognise and abide by the legal requirements associated with these rights.
• Users may download and print one copy of any publication from the public portal for the purpose of private study or research.
• You may not further distribute the material or use it for any profit-making activity or commercial gain
• You may freely distribute the URL identifying the publication in the public portal

Read more about Creative commons licenses: https://creativecommons.org/licenses/

Take down policy
If you believe that this document breaches copyright please contact us providing details, and we will remove access to the work immediately and investigate your claim.

LUND UNIVERSITY

PO Box 117
221 00 Lund
+46 46-222 00 00

Detailed Numerical Simulations of Turbulent Premixed Flames at Moderate and High Karlovitz Numbers

Henning Carlsson
December 2014

Thesis for the degree of Doctor of Philosophy in Engineering
ISSN 0282-1990
ISRN LUTMDN/TMHP-14/1106-SE
ISBN 978-91-7623-169-2 (print)
978-91-7623-170-8 (pdf)

©Henning Carlsson November 2014
Division of Fluid Mechanics
Department of Energy Sciences
Faculty of Engineering
Lund University
Box 118
SE-221 00 Lund
Sweden

Printed by Media-Tryck, Lund, November 2014.

Populärvetenskaplig Sammanfattning

Förblandad förbränning har sedan lång tid tillbaka varit en av grundbultarna i industriellt applicerad förbränning såsom i bensinmotorer och gasturbiner. Genom att direkt kunna kontrollera blandningsförhållandet mellan bränsle och luft kan utsläppen av skadliga ämnen hållas på en minimal nivå. Detta gör förblandad förbränning mycket attraktiv. För att industriellt applicerad förblandad förbränning ska kunna ge en signifikant effekt är det viktigt att förbränningen sker tillräcklig snabbt och därför används nästan alltid en turbulent omgivning, till exempel, i en bensinmotor måste allt bränsle brinna upp innan avgaserna trycks ut ur cylindern. För att på samma gång uppnå hög effekt, hög verkningsgrad och låga emissioner finns det en trend i industriella applikationer att gå mot allt magrare blandningsförhållanden och mer högintensiv turbulens. Växelverkan mellan flamma och turbulens vid dessa förhållanden är dock inte välförstådd och få numeriska modeller är utvecklade för att hantera denna typ av förbränning.

I denna avhandling används detaljerade numeriska simuleringar för att undersöka växelverkan mellan förblandade flammor och turbulens vid måttliga och höga turbulenta intensiteter. Direkt numerisk simulering (DNS) används för att studera grundläggande fysikaliska fenomen i högintensiva turbulenta flammor där samtliga skalor i både turbulens och detaljerad kemi är inkluderade med minimal modellering. Simuleringarna visar att på grund av ökad turbulent transport ökas mängden radikaler i lågtemperaturzonen i flamman, vilket i sin tur kan ge upphov till hög värmefrigörelse även vid låga temperaturer. Detta har aldrig påvisats vid låga turbulenta intensiteter. I och med att dessa fenomen uppstår från den komplicerade kemin som är involverad i förbränningsprocessen visar resultaten också att konventionell klassificering av turbulenta förblandade flammor inte kan förklara skillnaderna i radikallagrens växelverkan med turbulens mellan två studerade flammor. Ett nytt dimensionslöst tal definierades därför för att kunna ta effekter från detaljerad kemi i beaktande.

För studier av växelverkan mellan flamma och turbulens vid måttliga turbulenta intensiteter användes metoden large eddy simulation (LES) med en förbränningsmodell baserad på G-ekvationen. Denna förbränningsmodell är väl testad för mycket låga turbulenta intensiteter där turbulent transport inuti flamman är försumbar och i denna avhandling testades modellen för något högre turbulenta intensiteter. En experimentell brännare med tillgång på valideringsdata användes som testfall och med en dynamisk implementering av den lokala skrynklingen av flamman i förbrännings-

modellen uppvisade den mycket god jämförelse med den experimentella datan även vid relativt höga Reynolds tal. Modellen användes sedan för att studera växelverkan mellan flamma och frekvensspecifika koherenta strukturer där en vidareutvecklad version av dynamisk moduppdelning kunde hjälpa förståelsen för flammans stabiliseringsmekanism i den experimentella brännaren.

Abstract

In generally accepted and applied flamelet combustion models, a turbulent flame is mainly assumed distorted by the large-scale turbulence eddies, whereas small-scale turbulence effects on the local flamelet structures are neglected. However, in a lot of industrial applications rather high turbulent intensities are often imposed, which induce turbulence scales at ranges smaller than the flame thickness. Flame/turbulence interaction appears quite different at these small scales, which is why improvement of the combustion models is required to account for these phenomena.

In this thesis, direct numerical simulations (DNS) and large eddy simulations (LES) have been utilized for studies of lean premixed turbulent reactive flows at various turbulent intensities. DNS has been applied for detailed studies of flame-turbulence interaction to investigate flame structures and detailed chemistry effects at high Karlovitz numbers. Intensified convective-diffusive transport within the fine reaction zone layers is observed which is found to significantly alter the chemical pathway with, e.g., intensified heat release rate at low temperatures. Based on these observations a categorization, supplementary to the conventional one, is proposed, which is able to incorporate detailed chemistry effects into the classification of turbulent premixed flames at high Karlovitz numbers. The effect of differential diffusion was found significant, both globally (in terms of the fuel diffusion effect) and locally (in terms of the radical diffusion effect), also in the distributed reaction zone regime.

LES was employed for a low swirl stabilized flame utilizing a flamelet combustion model approach. A dynamic modeling approach to incorporate sensitivity to local variations in the subgrid scale flame wrinkling was implemented and validated. The simulations showed high sensitivity of the prediction of turbulent flame fluctuations as well as ambient air entrainment rate into burned gases to inflow conditions and operating conditions. Lower sensitivity was found to domain size and combustion model. Overall the model results showed good agreement with the velocity and scalar validation data in the thin reaction zone regime. In order to analyze the influence of frequency specific coherent structures on the flame dynamics extended dynamic mode decomposition was performed which was able to delineate the effects of the inner and outer shear layer vorticity on the flame stabilization.

List of Papers

I. J. Savre, **H. Carlsson**, X.S. Bai, Turbulent Methane/Air Premixed Flame Structure at High Karlovitz Numbers, *Flow Turb. Combust.* 90 (2013) 325-341.

II. **H. Carlsson**, R. Yu, X.S. Bai, Direct Numerical Simulation of Lean Premixed CH_4/Air and H_2/Air Flames at High Karlovitz Numbers, *Int. J. Hydrogen Energy*, in press (2014) DOI: 10.1016/j.ijhydene.2014.09.173.

III. **H. Carlsson**, R. Yu, X.S. Bai, Flame Structure Analysis for Categorization of Lean Premixed CH_4/Air and H_2/Air Flames at High Karlovitz Numbers: Direct Numerical Simulation Studies, *Proc. Combust. Inst.* in press (2014) DOI: 10.1016/j.proci.2014.09.002.

IV. A. Bohlin, E. Nordström, **H. Carlsson**, X.S. Bai, P.-E. Bengtsson, Pure Rotational CARS Measurements of Temperature and Relative O_2-concentration in a Low Swirl Turbulent Premixed Flame, *Proc. Combust. Inst.* 34 (2013) 3629-3636.

V. **H. Carlsson**, E. Nordström, A. Bohlin, P. Petersson, Y. Wu, R. Collin, M. Aldén, P.-E. Bengtsson, X.S. Bai, Large Eddy Simulations and Rotational CARS/PIV/PLIF Measurements of a Lean Premixed Low Swirl Stabilized Flame, *Combust. Flame* 161 (2014) 2539-2551.

VI. **H. Carlsson**, C. Carlsson, L. Fuchs, X.S. Bai, Large Eddy Simulation and Extended Dynamic Mode Decomposition of Flow-Flame Interaction in a Lean Premixed Low Swirl Stabilized Flame, *Flow Turb. Combust.* 93 (2014) 505-519.

Related Work

A. **H. Carlsson**, J. Savre, R. Yu, X.S. Bai, Combustion Regime Influences on Differential Diffusion and Reaction Progress in Lean Premixed Hydrogen/Air Flame: a Detailed Numerical Study, *7th Mediterranean Combustion Symposium*, *Paper TC-34*, Sardinia, Italy (2011).

B. P. Petersson, R. Wellander, J. Olofsson, **H. Carlsson**, C. Carlsson, B.B. Watz, N. Boetkjaer, M. Richter, M. Aldén, L. Fuchs, X.S. Bai, Simultaneous High-Speed PIV and OH PLIF Measurements and Modal Analysis for Investigating Flame-Flow Interaction in a Low Swirl Flame, *16th International Symposium on Applications of Laser Techniques to Fluid Mechanics*, Lisbon, Portugal (2012).

C. **H. Carlsson**, P. Petersson, C. Carlsson, R. Wellander, M. Richter, L. Fuchs, X.S. Bai, M. Aldén, Flame Speed Analysis in a Methane/Air

Low Swirl Premixed Flame, *6th European Combustion Meeting*, *Paper P4-63*, Lund, Sweden (2013).

D. H. Carlsson, R. Yu, M. Jangi, X.S. Bai, Enhanced Chemistry Coordinate Mapping Method with Error Control, *8th Mediterranean Combustion Symposium*, *Paper TC-12*, Çeşme, Turkey (2013).

Acknowledgements

This work was carried out at the division of Fluid Mechanics, department of Energy Sciences, Lund University, Sweden. The work was financially supported by the Swedish Research Council (VR) and the national Centre for Combustion Science and Technology (CeCOST). Computations were performed using computer facilities provided by the Centre for Scientific and Technical Computing at Lund University (LUNARC), High Performance Computing center North (HPC2N), and Center for Parallel Computers (PDC). I also acknowledge PRACE for awarding access to resources CURIE TN based in France at TGCC and SUPERMUC based in Germany at LRZ.

In the more personal part of this section I would like to start by thanking my supervisor Prof. Xue-Song Bai for providing me the opportunity of performing these PhD studies within his group. Thank you for valuable discussions, for being open to my ideas, and for sharing your knowledge on how to conduct research.

I gratefully thank my co-supervisors Dr. Rixin Yu and Prof. Laszlo Fuchs for all good ideas and input during our discussions. I thank my other collaborators who, with their work, helped improve the quality of mine. I want to especially mention Prof. Per-Erik Bengtsson, Dr. Alexis Bohlin, Dr. Christian Carlsson, Emil Nordström, and Dr. Yajing Wu for fruitful discussions.

The previous and current staff at the department of Energy Sciences deserves great acknowledgement for creating a nice work environment. By frequently attending the lunch tables, coffee breaks, and the pub some evenings I would like to especially mention Ali, Henrik, Hesam, Maria, and Parisa, but to the ones not mentioned by name I am not less grateful. Thank you all for the friendliness and the great spirit you have shown me.

I take the risk of balancing maybe too close to a bromance by dedicating a separate paragraph to Rickard Solsjö. We have studied and worked side by side for several years and you have throughout this time been a major support, for which I am eternally grateful.

In order to complete a doctoral thesis work it is very important to believe that it is possible, or at least have someone else who does. My final paragraph of this section I therefore dedicate to my parents Bernt-Ove and Karin and my brothers Magnus and Tommy for always believing in me also in times when I did not.

Contents

Nomenclature

Latin Characters

A	arbitrary operator [-]
A_L	instantaneous turbulent flame front area [m^2]
A_M	laminar flame area [m^2]
A_s	Arrhenius constant [depending on reaction]
C	companion matrix [-]
C_F	turbulent kinetic energy scaling factor [m^{-1}]
C_p	mixture averaged heat capacity at constant pressure [$J \cdot kg^{-1} \cdot K^{-1}$]
$C_{p,s}$	heat capacity of species s at constant pressure [$J \cdot kg^{-1} \cdot K^{-1}$]
C_s	Smagorinsky constant [-]
C_Ξ	wrinkling factor coefficient [-]
C_μ	turbulent viscosity constant in the RANS framework [-]
D	diameter [m]
$D_{f/a}$	mass diffusion coefficient for fuel-air mixture [$m^2 \cdot s^{-1}$]
D_s	mass diffusion coefficient for species s [$m^2 \cdot s^{-1}$]
D_0	mass diffusion constant [$kg \cdot m^{-1} \cdot s^{-1}$]
E	turbulent kinetic energy spectrum [$m^3 \cdot s^{-2}$]
E_a	activation energy [$J \cdot mole^{-1}$]
E_ψ	power density spectrum for variable ψ [varying]
F_Δ	filter function [m^{-3}]
$\mathcal{F}$	Fourier transform operator [-]
G	flame coordinate [m]
L_c	characteristic length scale [m]
L_{ij}	integral length scale in directions i and j [m]
N_{sp}	total number of species [-]
P	thermodynamic pressure [pa]
$\dot{Q}$	radiative heat transfer rate [$J \cdot m^{-3} \cdot s^{-1}$]
R_ψ	two point correlation function for variable ψ [varying]
$\Re$	universal gas constant [$J \cdot mole^{-1} \cdot K^{-1}$]
S	flame propagation speed [$m \cdot s^{-1}$]
S_{ij}	symmetric rate of strain tensor [$m \cdot s^{-1}$]
S_L	laminar flame speed [$m \cdot s^{-1}$]
S_{LES}	propagation speed of the LES filtered reaction front [$m \cdot s^{-1}$]

S_T	turbulent flame speed [m·s^{-1}]
T	temperature [K]
T_0	reference temperature [T_0 = 298 K]
U_c	characteristic velocity [m·s^{-1}]
$V_{s,j}$	diffusion velocity for species s in direction j [m·s^{-1}]
W_s	molar mass of species s [kg·mole^{-1}]
$\bar{W}$	mean molar mass of mixture [kg·mole^{-1}]
Y_s	mass fraction of species s
$Y_{s,0}$	mass fraction of species s in unburned gases at equilibrium [-]
$Y_{s,b}$	mass fraction of species s in burned gases at equilibrium [-]
$Y_{e,all}$	total mass fraction of element e [-]
Z	mixture fraction [-]
a	speed of sound in medium [m·s^{-1}]
c	reaction progress variable [-]
e_i	unit vector component i [-]
$f_{s,j}$	specific volume force acting on species s in direction j [N·kg^{-1}]
g_{ij}	velocity fluctuation correlation function for velocity fluctuation components i and j [-]
h	enthalpy [J·kg^{-1}]
k	wave number [m^{-1}]
$\boldsymbol{k}_s$	wave number vector [m^{-1}]
l	integral length scale [m]
n_c	sgs wrinkling factor model constant [-]
n_A	Arrhenius exponent [-]
n_i	flame normal component i [-]
n_D	heat and mass diffusion constant [-]
p	pressure [pa]
p_h	hydrodynamic pressure [pa]
p'	pressure correction [pa]
q_i	energy flux [J·m^{-1}·s^{-1}]
r	spatial distance [m]
r_i	distance vector component i [m]
t	time [s]
u_i	velocity component i [m·s^{-1}]
u_i'	velocity fluctuation of velocity component i [m·s^{-1}]
u_l', u'	integral scale velocity fluctuation [m·s^{-1}]

u'_{sgs}	sgs velocity fluctuation [m·s^{-1}]
v_i	characteristic velocity i [-]
$\boldsymbol{v}, \boldsymbol{w}$	vector fields [m·s^{-1}]
x_i	space coordinate in direction i [m]

Greek Characters

Δ	filter width [m]
Δt	CFD time step [s]
Δx	grid spacing [m]
Ξ	flame wrinkling factor [-]
Ξ_Δ	sgs flame wrinkling factor [-]
Ω	fuel/oxidizer reactivity [s^{-1}]
α	sgs wrinkling factor model constant [-]
α_s	ratio of laminar to turbulent species specific time scales for species s [-]
β	sgs wrinkling factor model constant [m·s^{-1}]
δ	Dirac delta function [-]
δ_{ij}	Kronecker delta [1 if $i = j$, else 0]
δ_L	laminar flame thickness [m]
ε	dissipation rate of turbulent kinetic energy per unit mass [m^2·s^{-3}]
$\boldsymbol{\zeta}, \boldsymbol{\xi}$	vector fields [m^3·s^{-1}]
η	Kolmogorov length scale [m]
ρ_0	density of unburned fuel air mixture [kg·m^{-3}]
λ	thermal heat conductivity [J·s^{-1}·m^{-1}·K^{-1}]
λ_e	eigenvalue related quantity [varying]
λ_f	Taylor length scale [m]
μ	dynamic viscosity [kg·m^{-1}·s^{-1}]
μ_Δ	turbulent viscosity [kg·m^{-1}·s^{-1}]
ν	kinematic viscosity [m^2·s^{-1}]
ν_T	turbulent kinematic viscosity [m^2·s^{-1}]
ρ	density [kg·m^{-3}]
σ	strain [s^{-3}]
σ_e	egenvalue [varying]
τ_c	chemical time scale [s]
τ_l	integral time scale [s]
τ_s^L	chemical time scale of species s [s]
τ_s^T	turbulent effective chemical time scale of species s [s]

τ_η	Kolmogorov time scale [s]
τ_{ij}	viscous stress tensor [kg·m^{-1}·s^{-2}]
ϕ	fuel/air mixture equivalence ratio [-]
φ	local equivalence ratio [-]
$\dot{\omega}_T$	heat release rate per unit volume [J·m^{-3}·s^{-1}]
$\dot{\omega}_s$	reaction rate of species s per unit volume [kg·m^{-3}·s^{-1}]

Non-dimensional Numbers

$Da = \frac{\tau_l}{\tau_c}$	Damköhler number
$Le_s = \frac{\lambda}{\rho C_p D_s}$	Lewis number of species s
$Ka = \frac{\tau_c}{\tau_\eta}$	Karlovitz number
$Ka_s = \frac{\tau_s^L}{\tau_\eta}$	species specific Karlovitz number
$Ma = \frac{U_c}{a}$	Mach number
$Re = \frac{\rho U_c L_c}{\mu}$	Reynolds number
$Re_T = \frac{u_l' \cdot l}{\nu}$	turbulent Reynolds number

Abbreviations

CDR	convection diffusion reaction
CFD	computational fluid dynamics
CFL	Courant-Friedrichs-Lewy
DCM	dynamic coefficient model
DMD	dynamic mode decomposition
DNS	direct numerical simulation
DVODE	double precision variable-coefficient ordinary differential equation
EDMD	extended dynamic mode decomposition
FFT	fast Fourier transform
GT	gas turbine
HAB	height above burner
HOT	higher order terms
HRR	heat release rate per unit mass [J·kg^{-1}]
IC	internal combustion
ILES	Implicit LES

JPDF	joint probability density function
LBL	Lawrence Berkeley national lab
LES	large eddy simulation
LU	Lund university
ODE	ordinary differential equation
RANS	Reynolds averaged Navier-Stokes equations
RCARS	rotational coherent anti-Stokes Raman spectroscopy
RMS	root-mean-square
PIV	particle image velocimetry
PLIF	planar LIF
SCM	static coefficient model
SGS	subgrid scale
SSM	scale similarity model
TVD	total variation diminishing
WENO	weighted essentially non-oscillating

Chemical Compounds

CH	hydrocarbon radical
CH_4	methane
CO	carbon monoxide
CO_2	carbon dioxide
CH_2O	formaldehyde
C_3H_8	propane
H	hydrogen atom
H_2	hydrogen
HO_2	hydrodioxide
H_2O	water
M	third body species
N_2	nitrogen
NO_x	nitrogen oxides
O	oxygen atom
O_2	oxygen
OH	hydroxide
UHC	unburned hydrocarbons

Chapter 1
Introduction

Combustable fuels have for a long time been the primary source of the human energy supply. At present time with an increasing living standard and a growing population of the planet earth, the energy demand is rising and combustion of fossil as well as renewable fuels will therefore be of high importance also in the future. To assure energy access at the same time as pollution limitations have to be met, comprehensive research within the field of combustion needs to be conducted. The important combustion emissions are unburned hydrocarbons (UHC), nitrogen oxides (NO_x), carbon monoxide (CO), and soot. UHC is not only a pollutant itself but high residues of unburned fuel also lower the efficiency of the combustion devices. UHC typically origins from regions where the flame is quenched or from fuel hiding at inflammable locations in the combustor. NO_x is a toxic gas that is formed primarily at high flame temperatures and CO is a toxic gas that is formed at low (or very high) flame temperatures. Soot is a collective term for larger (>10 nm) carbon-rich particles formed in fuel rich locations through chain reactions. The desire is of course to minimize all these emissions simultaneously, but also to maintain high combustion efficiency. This is important for economical reasons, but also since the combustion product CO_2 is a green house gas and the fuel consumption should be kept low in order to minimize the effect on the climate. Combustion control is therefore of major importance to ensure that the system operates at suitable conditions in terms of flame temperature, fuel/oxidizer composition, and flame/flow interaction.

Studies and development of combustion systems have for centuries been performed through experimental investigations where parameters have been tuned until desired features have been obtained. It was not until the invention of computers that computational fluid dynamics (CFD) became a scientific tool for studies of flows and combustion properties. As the computational power has become greater and cheaper, CFD has become applicable to industrial applications involving combustion where trends of e.g., changes of the geometry or the fuel composition can be determined without experiments. Especially in terms of the former, great economical benefits can be found. Instead of constructing several test vessels, the trends can be determined through CFD simulations at a much lower cost.

When CFD methods are utilized in industrial applications, usually through the Reynolds averaged Navier-Stokes (RANS) approach or large eddy simulations (LES), modeling difficulties to account for interaction of turbulent structures at scales much smaller than the laminar flame thickness arise. Due to complex flame/flow interaction at these scales [1] several phenomena, which are not well known, arise. For example, fuel diffusion characteristics can cause variations of the flame composition along the flame due to turbulence induced curvature, turbulence caused flame strain alters both structure and propagation speed of the flame, and at high straining, local flame extinction as well as re-ignition can occur [1]. These effects should ideally be accounted for in the employed combustion model. With acceptable accuracy the flames are often assumed undisturbed at small scales through utilization of so called flamelet models. This is not solely due to desired computational speed up, but also since well verified combustion models for the high intensity turbulence combustion regimes are lacking to this date. Flamelet models assume that composition and rates of a flame can be represented by a rather narrow manifold, which greatly simplifies the model. In an idealized case a flame can even be assumed to be represented by an iso-surface which is transported by convection and self-propagation. Modifications of these models can be made to account for e.g., local extinction to some extent; however, since the basic assumptions of the models are not valid in high turbulent intensity combustion regimes, a different approach is most likely a necessary option.

When models for the high intensity turbulence combustion regimes are to be developed, sufficient reference data is required. It is difficult to experimentally achieve high turbulent intensities in a laboratory combustion environment [2] and once it is obtained, simultaneous multi-species and temperature measurements are to be conducted. This demands access to complex and expensive equipment. Multi-species measurements in these types of flames have not been conducted until very recently [3-7], where a rather comprehensive set of radicals is shown in [6,7]. However, to obtain a complete picture, quantitative simultaneous scalar and reaction rate measurements in 3D are necessary. This is probably not feasible in the near future, which is why direct numerical simulations (DNS), due to the massive increase of computer power access during recent years, will play an important role as it is able to supply this kind of data with minimal modeling required.

The scope of this thesis is to apply CFD to studies of turbulent premixed combustion at moderate and high turbulent intensities, where the interaction

between a turbulent flow and a flame behaves quite different depending on the size and speed of the turbulence vortices. As mentioned above, premixed combustion is conventionally used in spark ignition engines and stationary gas turbines. This thesis is directly related to applications to gas turbines where swirl stabilized flames are successfully employed to achieve ultra-low emissions of NO_x. Practical difficulties still remaining are e.g., flashback, blow-off, thermo-acoustic oscillations, and combustion noise. Here the focus is not on these issues per se, but instead the modeling difficulties arising during simulations of these types of flames such as the application of flamelet models to flames in the thin-reaction zone regime. The experimental low swirl burner [8] is studied and used as validation case when employing LES with the flamelet G-equation model. The case is also used for studies of flame dynamics during interaction with coherent flow structures. New experimental data are used to evaluate the model performance.

DNS is employed for studies of flames that interact with very high intensity turbulence. These studies are directed towards an improved understanding of the underlying physics of the interaction between flames and intense turbulence. Neither the effects of detailed chemistry nor differential diffusion at such conditions are well understood. Furthermore, classification of turbulent premixed flames have been a subject of debate during the past decades (especially for the high intensity turbulence combustion regimes) and in this work, the effects of detailed chemistry is also incorporated in that discussion. Finally, large scale DNS are of course always valuable for providing data-bases for future model development and validation.

Following this short introduction, the theory of premixed turbulent combustion is summarized in chapter 2. The methods utilized are described in chapter 3. The high intensity turbulent flame DNS project is presented in chapter 4. The low swirl burner LES project is summarized in chapter 5. A summary of the papers, on which this thesis is based on, is given in chapter 6 along with outlined respective contribution by the candidate. Chapter 7 contains relevant conclusions and an outlook towards future work. Further details of the results are given in the papers listed in the appendix.

Chapter 2
Turbulent reactive flows

2.1 Turbulence

2.1.1 Laminar and Turbulent Flows

Turbulent flows are characterized by irregularity, randomness, and chaos, where the turbulence, through turbulent diffusion, greatly increases the mixing within a fluid compared with laminar flows. Laminar flows are characterized by streamlines of parallel layers and a transport in the transversal direction to the flow direction that is simply governed by viscous diffusion. In most industrial applications mixing needs to be fast and the flows are therefore usually kept turbulent. Turbulence is often characterized using the Reynolds number [9]:

$$Re = \frac{\rho U_c L_c}{\mu}\,, \tag{1}$$

where ρ is density, U_c is a characteristic velocity, L_c is a characteristic length scale, and μ is dynamic viscosity. The Reynolds number is given by the ratio between inertial forces and viscous forces and roughly characterizes the flow independently of fluid or geometry. Turbulent flows are associated with large Reynolds numbers.

2.1.2 Scales of Turbulence

Turbulent kinetic energy cascading is of central importance in turbulence theory. Richardson stated the first turbulence concept [10], where turbulence can be considered composed of turbulence eddies of different sizes. The length scale of the large scale motion is on the same order as the apparatus generating the turbulence, and turbulent kinetic energy is thereafter cascaded from larger to smaller scales until finally dissipated by viscosity at the smallest scales. For characterization of turbulence scales in homogeneous turbulence, the correlation function for velocity fluctuation u_i' can be defined as:

$$g_{ij}(\boldsymbol{r}) = \frac{\langle u_i'(\boldsymbol{x}) u_j'(\boldsymbol{x}+\boldsymbol{r})\rangle}{\langle u_i'(\boldsymbol{x}) u_j'(\boldsymbol{x})\rangle}, \tag{2}$$

where $\langle\cdot\rangle$ denotes ensemble, time, or volume averaging, and $\boldsymbol{r}$ is a distance vector from position $\boldsymbol{x}$. The integral length scale, l, describing the large scale structures, is defined through integration of this autocorrelation function:

$$l = L_{11} = \int_0^\infty g_{11}(\boldsymbol{e}_1 \cdot r)dr, \tag{3}$$

where L_{ij} is a directional integral length scale and $\boldsymbol{e}_i$ is the unit vector in the x_i-coordinate direction. At this scale, the characteristic velocity (u_l', or simply u', which is often referred to as turbulent intensity) is a very important property for characterization of turbulence. Based on these length and velocity scales a turbulent Reynolds number is also defined:

$$Re_T = \frac{u_l' l}{\nu}, \tag{4}$$

where ν is kinematic viscosity.

For a Reynolds number that is large enough, in-between the smallest and largest scales of turbulence there is a cascading range where energy is transferred from larger to smaller scales. This range is commonly referred to as the inertial sub-range, for which it can be shown [11] that the following relation for distribution of turbulent kinetic energy amongst scales, $E(k)$, holds:

$$E(k) \propto \varepsilon^{2/3} k^{5/3}, \tag{5}$$

where ε is dissipation rate and k is wave number. Related to this range is the Taylor scale, λ_g. This scale is also based on the autocorrelation function $g_{ij}(\boldsymbol{r})$ and defined through:

$$\lambda_g = \left(-\frac{1}{2} \frac{d^2 g_{11}(\boldsymbol{e}_1 \cdot 0)}{dr^2} \right)^{-1/2}. \tag{6}$$

The Taylor scale has no obvious physical interpretation, but it is commonly used to estimate the inertial sub-range [11].

Later, in two similarity hypotheses from Kolmogorov [12], the turbulence theory for small scale turbulence was stated. The small scales of turbulence are solely governed by the kinematic viscosity and the rate of dissipation. Based on these two quantities, through dimension analysis, the Kolmogorov length and time scales were defined:

$$\begin{aligned} \eta &= (\nu^3/\varepsilon)^{1/4} \\ \tau_\eta &= (\nu/\varepsilon)^{1/2}, \end{aligned} \tag{7}$$

which are respectively the characteristic length and time scales of the smallest scales of turbulence. By assuming $\varepsilon \sim u'^3/l$, the Kolmogorov length scale can be estimated through the turbulent Reynolds number:

$$\eta = \frac{l}{Re_T^{3/4}}. \tag{8}$$

A schematic sketch of an energy spectrum for a homogeneous high Reynolds number turbulent flow is shown in Fig. 2.1.

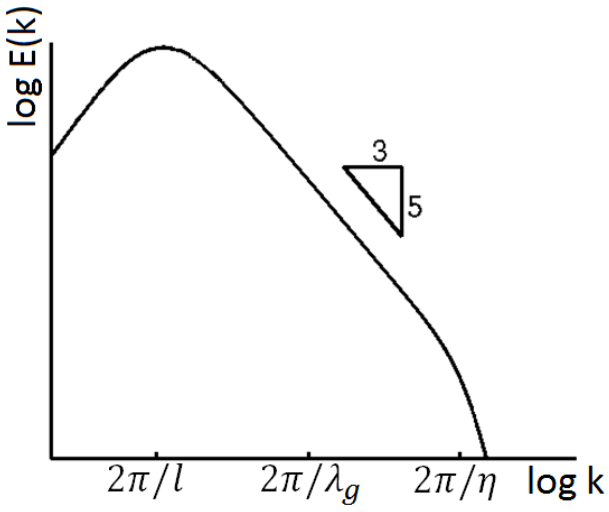

Figure 2.1. Turbulent kinetic energy spectrum as function of wave number.

This type of turbulence is theoretical and may be termed “Kolmogorov turbulence”. The turbulence found in most practical application does not follow this theory, and are not fully homogenous and isotropic.

2.2 Combustion

2.2.1 Premixed and Non-premixed Combustion

Combustion is a collective term for all types of exothermic reaction processes where fuel is oxidized and heat is released. Combustion is generally divided into two large classes: non-premixed and premixed combustion.

In non-premixed combustion fuel and oxidizer are separated prior to reaction and are later reacting simultaneous with the mixing process. The reaction is taking place around stoichiometric proportions with high flame temperature and the flame is governed by chemical reactions as well as diffusion and turbulent mixing (in case of a turbulent environment). The temperature of a non-premixed flame is therefore difficult to control and may lead to high emissions of NO_x. On the other hand, non-premixed flames also provide desirable characteristics; they are easy to stabilize and the separation of fuel and oxidizer prior to combustion makes the practical handling of the combustion system rather secure. Common applications for non-premixed flames are candles, solid combustion, rocket engines, aero-engines, and diesel engines.

In premixed combustion the fuel and oxidizer are mixed prior to reaction. Contrary to non-premixed flames, premixed flames have a distinct reaction zone with characteristics such as a laminar flame thickness and flame speed. Premixed combustion allows direct control of the flame temperature through the mass ratio between the fuel and the oxidizer in the mixture and thereby control of emissions. On the other hand, premixing gives rise to problems of stabilization, blow-off, and flashback. Common applications for premixed flames are Bunsen burners, spark-ignition engines, and stationary gas turbines.

2.2.2 Turbulent Premixed Combustion

As previously mentioned, in laminar premixed flames the flame is characterized by a laminar flame thickness, δ_L, and a laminar flame speed, S_L. For hydrocarbon fuel/air mixture at stoichiometric proportions and room

conditions the laminar flame speed is typically on the order of half a meter per second. This speed is far too low to be useful in industrial applications, which is why most combustion systems operate at turbulent conditions. Turbulence wrinkles the flames and increases the flame area and thereby the fuel consumption speed. To quantify the fuel consumption speed a turbulent burning velocity, S_T, can be defined through a relation with flame area:

$$S_T = A_L/A_M \cdot S_L = \Xi \cdot S_L, \tag{9}$$

where A_L is an instantaneous turbulent flame front area, A_M is the corresponding mean turbulent flame area, and Ξ is a flame wrinkling factor. In applied turbulent premixed combustion the mean flame is therefore propagating at a much higher velocity than a corresponding laminar flame ($S_T \sim 10 \cdot S_L$). This relation is shown in a schematic sketch in Fig. 2.2. However, as described in Section 2.1, turbulence consists of a range of turbulence scales. Flame wrinkling is mainly conducted by the highly energetic large scale eddies, whereas the small scale eddies can cause different types of interaction with the flame depending on their length and time scales. To show the inner structures of a premixed flame, a 1D flame profile for a lean methane/air flame computed with the Smooke-Giovangigli mechanism [13] is presented in Fig. 2.3. Here it can be seen that the flame profile can be divided into a preheat zone, a fuel-consumption zone (inner layer [14]), and an oxidation zone. The temperature in the preheat zone is raised mainly due to diffusion of heat from the reaction zone and not due to significant heat release rate. The fuel-consumption zone is a thin layer where the fuel and the oxidizer are consumed through several chain branching and chain propagating reactions involving intermediate radicals

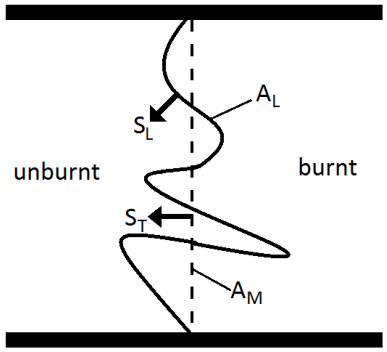

Figure 2.2. Flame wrinkling by turbulence shown schematically.

such as: H, O, OH, CH, and CH_2O for hydrocarbon flames. The oxidation zone is following the fuel-consumption zone and the remaining heat is released through oxidation of intermediate species (e.g., H_2 and CO). Relative to the fuel-consumption zone, the oxidation zone is wider and thereafter equilibrium burned gases are reached quite far downstream, cf. Fig. 2.3.

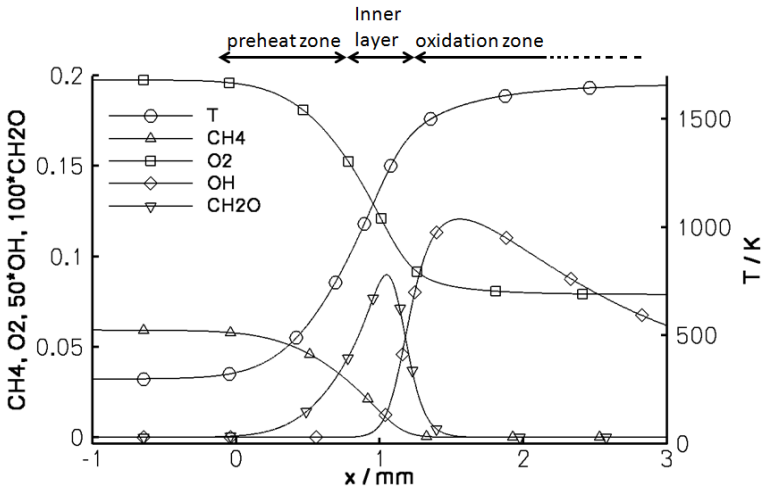

Figure 2.3. Flame structure of a lean premixed methane/air flame at equivalence ratio $\phi = 0.62$ and room conditions computed with Smooke mechanism [13].

To describe the interaction of turbulence with premixed flames, the turbulent Reynolds number can be expressed based on the characteristic flame properties, S_L and δ_L. In a laminar flame, since flame propagation and flame width are depending on reaction and diffusion rates of the flame, the following estimation can be made:

$$S_L \sim \sqrt{D_{f/a} \cdot \Omega}, \qquad \delta_L \sim \sqrt{D_{f/a}/\Omega}$$
$$S_L \cdot \delta_L \sim D_{f/a} \sim \nu$$
$$Re_T \approx \frac{u_l' \cdot l}{S_L \cdot \delta_L}, \tag{10}$$

where Ω is fuel/oxidizer reactivity and $D_{f/a}$ is the mass diffusivity of the fuel-air mixture. The interaction between small scale turbulence and a flame is quantified through the Karlovitz number:

$$Ka = \frac{\tau_c}{\tau_\eta} \sim \left(\frac{u_l'}{S_L}\right)^{3/2} \left(\frac{\delta_L}{l}\right)^{1/2} \sim \left(\frac{\delta_L}{\eta}\right)^2, \quad (11)$$

where τ_c is the chemical time scale and τ_η is the Kolmogorov time scale. As seen in the right hand side expression of Eq. (11) the Karlovitz number behaves as the ratio between the laminar flame thickness and the Kolmogorov length scale squared. A Karlovitz number of unity therefore means that the flame thickness and the smallest scale of turbulence are of the same order and a Karlovitz number of 100 means that the smallest scale of turbulence is about one order of magnitude smaller than the flame thickness. This is typically the width of the inner reaction zone layer. In addition to the Karlovitz number, the Damköhler number is sometimes used for categorization of turbulent premixed flames. The Damköhler number is defined based on the integral time scale, τ_l, and has also an inverse relation between turbulence and chemistry time scales compared with the Karlovitz number. The Damköhler number is defined as:

$$Da = \frac{\tau_l}{\tau_c}. \quad (12)$$

The turbulent premixed combustion diagram proposed by Borghi [15] and later revised by Peters [16] is a generally accepted description of eddy/flame interaction in premixed flames. The Peters-Borghi diagram is shown in Fig. 2.4, where the different combustion regimes and operating ranges for industrial internal combustion (IC) engines and aero gas turbine engines (GT) [17] are marked. As the trend in these industrial applications is to utilize leaner mixtures and higher turbulent intensities, the overall tendency of these operating ranges are towards higher Karlovitz numbers. This trend is marked in Fig. 2.4 with arrows. Furthermore, the turbulent flames studied in this thesis work have also been marked in Fig. 2.4. In the Peters-Borghi diagram, laminar flames are defined for turbulent Reynolds numbers smaller than unity. When the Karlovitz number is smaller than one, the flame is considered a flamelet as it is solely influenced by turbulence at scales that are larger than the flame thickness, which means that the flame can be locally approximated as one-dimensional (if differential diffusion is neglected). Extensive experimental [5,6,18-20] and numerical [16,21-23] investigations have been dedicated to study flames in the flamelet regime

showing results consistent with theory and the flamelet regime can be considered rather well understood [24].

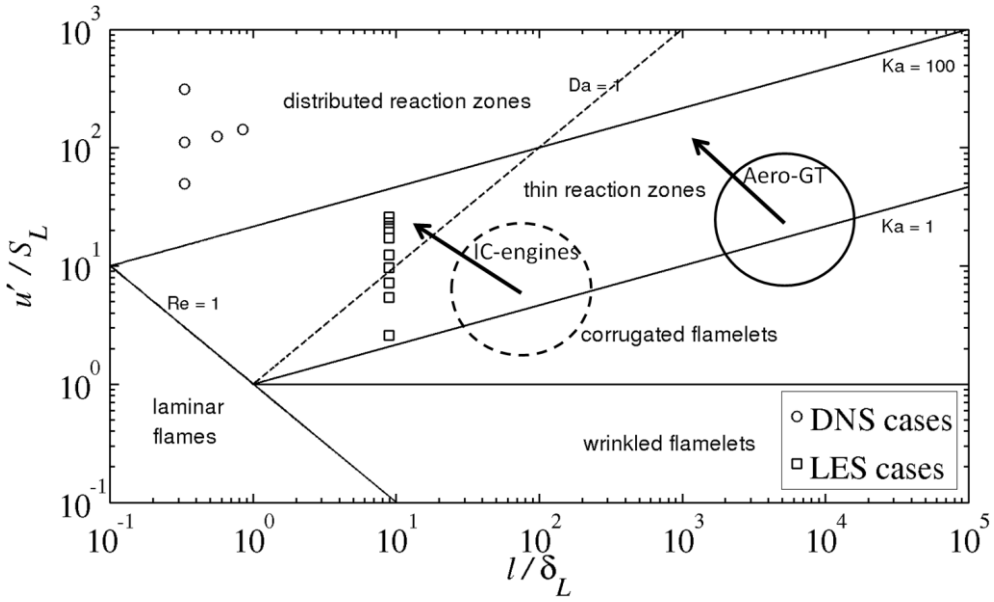

Figure 2.4. Premixed turbulent combustion regime diagram.

According to theory, for Karlovitz numbers greater than one, the smallest scales of turbulence are able to penetrate into the flame preheat zone and cause preheat zone broadening. This combustion regime is called the thin reaction zone regime since turbulence should not be able to penetrate the thin inner reaction zone layer and the thin reaction zone is thereby intact. Preheat zone broadening has been shown experimentally [5,6,25,26] as well as numerically [27,28] and can be considered a well known feature. However, the effect of preheat zone broadening on the turbulent burning rate is a less known phenomenon. During modeling of premixed flames in the thin reaction zone regime, the flamelet concept is often extended to be assumed valid at quite large Karlovitz numbers. The preheat zone is disturbed; however, since the inner reaction zone should be left unperturbed, flamelet models are often, with great success, also applied in this combustion regime. When the Karlovitz number is greater than 100 the smallest scales of turbulence are also smaller than the inner reaction zone layer and an unproven hypothesis of this combustion regime is therefore that increased mixing inside the inner reaction zone layer can cause flame

quenching [16]. This combustion regime was referred to as the broken reaction zone regime by Peters [16], but is commonly also referred to as the distributed reaction zone regime.

Flame quenching has been shown experimentally in jet flames [3-6,29]; however, whether the quenching was caused by turbulence straining or rapid entrainment of cooling air to the flame could not be concluded. It should also be pointed out that the limit of Karlovitz number 100 that separates the thin-reaction zone regime from the distributed reaction zone regime can be considered highly theoretical. First, the Kolmogorov length scale is within an order of magnitude from the smallest eddy in a turbulence field and the argument that the smallest eddies in the turbulence field is smaller than the inner layer of the flame is not necessarily fulfilled at Ka = 100. Second, viscosity increase across a flame greatly raise the Kolmogorov length scale, which questions if the small scale turbulence structures survive for a sufficient time to cause the kind of expected interaction with the inner reaction zone layer before they are dissipated. Fundamental questions such as what can be considered distributed combustion, if distributed burning is reached, and what kind of flame characteristics that can be found in the distributed reaction zone regime are of great importance for modeling of combustion systems where distributed burning is expected to occur, e.g., in large scale industrial gas turbines at high load [30].

It is difficult to reach well defined high turbulent intensities in laboratory experimental rigs. Strakey et al. [31] showed in experiments of a swirl burner u'/S_L on the order of 150, which is fairly high; however, the measurements were performed for a non-reacting flow field and to quantify the exact conditions of the turbulence that interacts with the flame is challenging. Due to such challenges as well as the requested quantities for a comprehensive understanding (c.f. Chapter 1), DNS has risen as a suitable tool for detailed studies of flame-turbulence interaction at well defined conditions. Structures of flames in the distributed reaction zone regime were investigated by Poludnenko and Oran [28] as dependant on resolution by utilizing a simplified chemistry model. Effects of both small and large turbulence scales on the flame were found highly resolution dependant and it was concluded that in their case, turbulence scales much smaller than the laminar flame thickness did not play a prominent role in terms of the effect on the flame brush properties and dynamics.

Figure 2.4 implies that the effect of different fuels does not need to be explicitly accounted for as it is already implicitly included through the

influence of the fuel properties on S_L and δ_L. However, due to differences in mass diffusion speed relative to thermal diffusion speed the combustion in multi-dimensional systems can appear quite different for different fuels. The ratio is presented through the Lewis number, Le_s:

$$Le_s = \frac{\lambda}{\rho C_p D_s}, \tag{13}$$

where λ is the mixture averaged thermal conductivity, C_p is the mixture averaged heat capacity at constant pressure, and D_s is the mass diffusion coefficient for species s. Non-unity Lewis number will cause significant influence to the flame shape. Several species, O_2, N_2, CH_4, CO, CO_2, and H_2O, have Lewis numbers close to unity and can therefore, for simplification, be assumed to be unity. However, other important species, e.g., H, H_2, and C_3H_8, have a Lewis number quite far from unity, for which the same simplification cannot be made that easily. When flame curvature and species and temperature gradients appear (which they do at a flame front), non-unity Lewis number has an influence on the flame structure. Due to these gradients species and temperature diffuse in the opposite direction to the gradient at different speed relative to each other. This effect is referred to as differential diffusion. The equivalence ratio will therefore be locally different at different positions within the flame. The latter effect is not a problem to model when a flamelet concept is used. However, flame curvature is also induced in turbulent flames. The multi-dimensional effect of differential diffusion will then cause focusing of rapidly diffusing species ($Le_s < 1$) in convex flame regions and defocusing in concave regions and vice versa for slowly diffusing species ($Le_s > 1$) [32,33]. This effect is difficult to capture by applying the flamelet concept and to scrutinize its influence during interaction with turbulence, high resolution numerical studies need to be performed.

For quantification of differential diffusion a local equivalence ratio, φ, is often computed. For a hydrocarbon fuel it can be expressed as [34]:

$$\varphi = \frac{\frac{Y_{\mathrm{H},all}}{2 \cdot W_{\mathrm{H}}} + \frac{2 \cdot Y_{\mathrm{C},all}}{W_{\mathrm{C}}}}{\frac{Y_{\mathrm{O},all}}{W_{\mathrm{O}}}}, \tag{14}$$

where $Y_{\mathrm{H},all}$ is the mass fraction of hydrogen element, W_{H} is molar mass of the hydrogen atom, $Y_{\mathrm{C},all}$ is mass fraction of the carbon element, W_{C} is molar mass of the carbon atom, $Y_{\mathrm{O},all}$ is mass fraction of the oxygen element, and W_{O} is molar mass of the oxygen atom. Aspden et al. [35-38] have in several publications studied Lewis number effects in flames in the distributed reaction zone regime. It was shown that the effect of differential diffusion both in the normal direction as well as the tangential direction of the flame was greatly reduced at high Karlovitz numbers. The turbulent intensity was maintained using a density weighted forcing algorithm and chemistry was considered using detailed mechanisms.

In a turbulent flame it is necessary to express reaction progress for quantification of the flame structure. As previously described, the fuel Lewis number can differ a lot and when defining a reaction progress variable, c, based on the fuel species this effect is important to bear in mind. c is defined as:

$$c(\boldsymbol{x},t) = \frac{Y_{f,0} - Y_f(\boldsymbol{x},t)}{Y_{f,0} - Y_{f,b}}, \tag{15}$$

where $Y_{f,0}$ is the fuel mass fraction in the unburned mixture, Y_f is the local mass fraction of fuel, and $Y_{f,b}$ is the fuel mass fraction in the burned mixture at equilibrium.

2.3.3 Mathematical Description

For Newtonian fluids the flow is governed by conservation equations for total mass (the continuity equation) and momentum (the Navier-Stokes equations). In conserved form these equations can be written [21]:

$$\frac{\partial \rho}{\partial t} + \frac{\partial \rho u_i}{\partial x_i} = 0 \tag{16}$$

$$\frac{\partial \rho u_i}{\partial t} + \frac{\partial \rho u_j u_i}{\partial x_j} = -\frac{\partial p}{\partial x_j} + \frac{\partial \tau_{ij}}{\partial x_j} + \rho \sum_{s=1}^{N_{sp}} Y_s f_{s,j}, \tag{17}$$

where u_i is the velocity component along the x_i direction, p is pressure, τ_{ij} is the viscous tensor, Y_s is the mass fraction of species s, N_{sp} is the number

of species, and $f_{s,j}$ is the specific volume force acting on s in the x_j direction. Pressure is determined through the equation of state:

$$p = \rho \Re T \sum_{s=1}^{N_{sp}} \frac{Y_s}{W_s}, \tag{18}$$

where $\Re$ is the universal gas constant, T is temperature, and W_s is the molar mass of species s. The viscous stress tensor is defined as:

$$\tau_{ij} = \mu \left(\frac{\partial u_i}{\partial x_j} + \frac{\partial u_j}{\partial x_i} - \frac{2}{3} \frac{\partial u_k}{\partial x_k} \delta_{ij} \right), \tag{19}$$

where δ_{ij} is the Kronecker delta.

In a reacting flow system, additional governing equations are the conservation equations for energy and species. Energy can be expressed either in terms of internal energy, enthalpy, or temperature. The different options have different advantages and disadvantages. Through the use of enthalpy in the energy equation, reaction rates are not explicitly accounted for in the equation since enthalpy is conserved during reaction. On the other hand temperature is a commonly used quantity, and relatively easily measured. The enthalpy equation can be written [21]:

$$\frac{\partial \rho h}{\partial t} + \frac{\partial \rho u_j h}{\partial x_j} = \frac{\partial p}{\partial t} + \frac{\partial u_j p}{\partial x_j} - \frac{\partial q_j}{\partial x_j} + \tau_{ij} \frac{\partial u_i}{\partial x_j} + \dot{Q} + \rho \sum_{s=1}^{N_{sp}} Y_s f_{s,j} V_{s,j}, \tag{20}$$

where q_j is the energy flux, $\dot{Q}$ is the heat source term, and $V_{s,j}$ is the diffusion velocity for species s in the x_j direction. The heat source term, e.g., due to spark ignition or radiative heat transfer, can be given explicitly.

Rewriting the energy equation in temperature form gives the conservation equation for energy in terms of temperature [21]:

$$C_p \frac{\partial \rho T}{\partial t} + C_p \frac{\partial \rho u_j T}{\partial x_j} = \frac{\partial p}{\partial t} + \frac{\partial u_j p}{\partial x_j} + \frac{\partial}{\partial x_j} \lambda \frac{\partial T}{\partial x_j} - \left(\rho \sum_{s=1}^{N_{sp}} C_{p,s} Y_s V_{s,j} \right) \frac{\partial T}{\partial x_j}$$

$$+\tau_{ij}\frac{\partial u_i}{\partial x_j} + \dot{Q} + \rho\sum_{s=1}^{N_{sp}} Y_s f_{s,j} V_{s,j} + \dot{\omega}_T, \qquad (21)$$

where $C_{p,s}$ is the specific heat capacity for species s at constant pressure and $\dot{\omega}_T$ is the heat release rate. The conservation equation for mass fraction of species s, Y_s, can be written [21]:

$$\frac{\partial \rho Y_s}{\partial t} + \frac{\partial}{\partial x_j}\left(\rho\left(u_j + V_{s,j}\right)Y_s\right) = \dot{\omega}_s, \qquad (22)$$

where $\dot{\omega}_s$ is the reaction rate of species s. The species mass diffusion, $V_{s,j}Y_s$, which appears in both energy and species equations, is often modeled using Fick's law:

$$-V_{s,j}Y_s = D_s\frac{\partial Y_s}{\partial x_j} - Y_s\sum_{i=1}^{N_{sp}} D_i\frac{\partial Y_i}{\partial x_j} + \frac{Y_s}{\bar{W}}\left(D_s - \sum_{i=1}^{N_{sp}} Y_i D_i\right)\frac{\partial \bar{W}}{\partial x_j} \qquad (23)$$

where $\bar{W}$ is the mean molar mass of the mixture. The last term in Eq. (23) appears due to the use of Fick's law based on mass fraction. This term is however negligible in mixtures with low spatial variation of $\bar{W}$, e.g., in nitrogen dominated systems such as premixed fuel/air combustion.

Chapter 3
Methods

3.1 Turbulence Modeling

3.1.1 Direct Numerical Simulation (DNS)

By definition there is no turbulence model employed in DNS. The full ranges of spatial and temporal scales are resolved, from the integral scale to the Kolmogorov scale, so that both turbulence cascading and dissipation on small scales can be physically accounted for without modeling. A very fine mesh is typically needed to assure that the Kolmogorov scales are resolved and DNS is therefore usually, due to heavy demands on computational resources, limited to small computational domains and low Reynolds numbers. With the present computational power DNS is rarely applied to industrial applications; however, for fundamental research DNS remains a useful tool for detailed studies of, e.g., autoignition events and flame/flow interaction [28,36,39-41]. A recent review on large scale DNS is given in [42]. In this thesis DNS has been employed for studies of high Karlovitz number effects in premixed flames.

3.1.2 Large Eddy Simulation (LES)

Within the framework of numerical simulations, LES is a more suitable approach to account for the transient and highly dynamic flow physics in full scale turbulent reacting application systems. In LES a coarser grid than in DNS is used such that the spatial resolution is within the inertial sub-range and (much) larger than the Kolmogorov scale. The small turbulence scales are responsible for the dissipation of turbulent kinetic energy and in LES these scales are assumed to be local and isotropic [43] and that their effect can be modeled. According to the standard turbulence spectrum (schematically displayed in Fig. 2.1) the main part of the turbulent kinetic energy is contained in the large scales and the concept of LES is therefore to resolve those large scales that contains the energetic dynamic flow features. In LES a spatially filtered form of the governing equations are solved with an LES filter size, Δ, usually on the grid resolution scale. The filter, denoted by over-bar, is defined here for a general function $\psi(\boldsymbol{x})$:

$$\bar{\psi}(\boldsymbol{x}) = \int \psi(\boldsymbol{x}')F_{\Delta}(\boldsymbol{x} - \boldsymbol{x}')d\boldsymbol{x}', \tag{24}$$

where F_{Δ} is a filter function. In general, the density is not constant in reacting flows and Favre filtering (denoted by over-tilde) is often used to derive a simplified form of the governing equations using the filtered variable,

$$\tilde{\psi} = \frac{\overline{\rho\psi}}{\bar{\rho}}. \tag{25}$$

By assuming a low Mach number (Ma) flow, neglecting viscous damping and radiation heat transfer, assuming a unity Lewis number for all species, and without volume forces, the filtered governing equations can be written:

$$\frac{\partial\bar{\rho}}{\partial t} + \frac{\partial\bar{\rho}\tilde{u}_i}{\partial x_i} = 0 \tag{26}$$

$$\frac{\partial\bar{\rho}\tilde{u}_i}{\partial t} + \frac{\partial\bar{\rho}\tilde{u}_j\tilde{u}_i}{\partial x_j} = -\frac{\partial\bar{p}}{\partial x_i} + \frac{\partial}{\partial x_j}\left(\tilde{\tau}_{ij} - \bar{\rho}\left(\widetilde{u_i u_j} - \tilde{u}_i\tilde{u}_j\right)\right) \tag{27}$$

$$\frac{\partial\bar{\rho}\tilde{h}}{\partial t} + \frac{\partial\bar{\rho}\tilde{u}_j\tilde{h}}{\partial x_j} = \frac{\partial}{\partial x_j}\lambda\left(\frac{\partial\tilde{h}}{\partial x_j}\right) - \frac{\partial}{\partial x_j}\left(\bar{\rho}\left(\widetilde{u_j h} - \tilde{u}_j\tilde{h}\right)\right) \tag{28}$$

$$\frac{\partial\bar{\rho}\tilde{Y}_s}{\partial t} + \frac{\partial\bar{\rho}\tilde{u}_j\tilde{Y}_s}{\partial x_j} = -\frac{\partial\bar{\rho}\widetilde{V_{s,j}Y_s}}{\partial x_j} - \frac{\partial}{\partial x_j}\left(\bar{\rho}\left(\widetilde{u_j Y_s} - \tilde{u}_j\tilde{Y}_s\right)\right) + \bar{\dot{\omega}}_s, \tag{29}$$

where $\tilde{\tau}_{ij}$ is the filtered rate-of-strain tensor,

$$\tilde{\tau}_{ij} = \mu\left(\frac{\partial\tilde{u}_i}{\partial x_j} + \frac{\partial\tilde{u}_j}{\partial x_i} - \frac{2}{3}\frac{\partial\tilde{u}_k}{\partial x_k}\delta_{ij}\right). \tag{30}$$

The Mach number is defined as:

$$Ma = \frac{U_c}{a} \tag{31}$$

where a is the speed of sound.

3.1.3 Subgrid Models for LES

For closure of the filtered LES equations, the subgrid transport terms $\bar{\rho}\left(\widetilde{u_i u_j} - \tilde{u}_i \tilde{u}_j\right)$, $\bar{\rho}\left(\widetilde{u_j h} - \tilde{u}_j \tilde{h}\right)$, and $\bar{\rho}\left(\widetilde{u_j Y_s} - \tilde{u}_j \tilde{Y}_s\right)$ and the filtered reaction rate term $\bar{\dot{\omega}}_s$ need to be modeled. A large number of models for the subgrid (SGS) transport terms have been developed through the years, e.g., the Smagorinsky model [44], the one-equation model [45,46], the scale similarity model [47], and the Germano dynamic model [48]. Throughout this thesis work, the Smagorinsky model and the scale similarity model as well as the concept of implicit LES (ILES) (where an explicit model is not used at all) have been employed.

3.1.3.1 Smagorinsky Model

The Smagorinsky model is an eddy-viscosity model where the effect of the SGS terms is simply modeled as an increased turbulent viscosity, μ_Δ. The effect of the SGS-term in Eq. (27) is therefore modeled in analogy with Eq. (30):

$$\bar{\rho}\left(\widetilde{u_i u_j} - \tilde{u}_i \tilde{u}_j\right) = \mu_\Delta \left(\frac{\partial \tilde{u}_i}{\partial x_j} + \frac{\partial \tilde{u}_j}{\partial x_i} - \frac{2}{3} \frac{\partial \tilde{u}_k}{\partial x_k} \delta_{ij} \right). \tag{32}$$

Modeling of the turbulent viscosity is similar as using the Boussinesq's hypothesis in the RANS framework and has been directly extrapolated for LES:

$$\mu_\Delta = \bar{\rho} (C_S \cdot \Delta)^2 \sqrt{2 \tilde{S}_{ij} \tilde{S}_{ij}}, \tag{33}$$

where C_S is the Smagorinsky constant and $\tilde{S}_{ij}$ is the filtered symmetric rate of strain tensor. The Smagorinsky model is very commonly applied in LES due to its simplicity as well as its consistent asymptotic behavior as the grid is refined ($\mu_\Delta \propto \Delta^2$). The main drawbacks of the Smagorinsky model is that the Smagorinsky constant is not uniquely defined and conventional usage (C_S = 0.17) sometimes overpredicts the dissipation on small scales. Furthermore, μ_Δ is always positive, which does not allow for back-scattering (reversed energy cascading from small to large scales) by the model.

3.1.3.2 Scale Similarity Model (SSM)

Similar to the Smagorinsky model, modeling of unclosed terms with SSM is directly based on the resolved filtered variables; however, unlike the Smagorinky model SSM is not an eddy-viscosity based model. The underlying assumption of SSM is that, due to the self-similar state of turbulence cascading and LES filtering on the inertial sub-range, the unresolved scales should behave similar as the resolved scales. A test filter is therefore employed to the Favre-filtered variables (denoted by hat) at a scale larger than the LES filter. For a variable ψ SSM gives:

$$\bar{\rho}\left(\widetilde{u_j\psi} - \tilde{u}_j\tilde{\psi}\right) \approx \bar{\rho}\left(\widehat{\tilde{u}_j\tilde{\psi}} - \hat{\tilde{u}}_j\hat{\tilde{\psi}}\right). \tag{34}$$

This model is directly applicable to all unclosed terms in Eqs. (27-29). Unlike the Smagorinsky model, SSM does not limit the unclosed term to be solely positive and backscattering from small scale to large scales can be somewhat accounted for. The disadvantage of this model is that it generally underpredicts the dissipation rate of ψ, which can lead to numerical instabilities of the system.

3.1.3.3 Implicit LES (ILES)

In the concept of ILES the unclosed terms are simply neglected, which is commonly referred to as "handled implicitly". Instead of an explicit SGS model, ILES relies on an appropriate dissipation due to the employed numerical scheme. If the lowest order truncation error term induced by the discretization scheme employed to the convective term in the momentum equation has an even order derivative, e.g.,

$$\frac{\partial u_i}{\partial x} = \frac{u_i^{n+1} - u_i^n}{\Delta x} - \frac{\Delta x}{2}\frac{\partial^2 u_i}{\partial x^2} + \text{HOT}, \tag{35}$$

the lowest order term in the truncation error behaves as a dissipating diffusion term [49-51]. In Eq. (35), the superscript n denotes the grid cell integer index, Δx is the grid size, and HOT is higher order terms.

3.2 Combustion Modeling

Combustion modeling is an expression which is not uniquely defined in terms of terminology. Generally it means determination of the heat release rate and species reaction rates in Eqs. (21-22) or determination of the filtered species reaction rates in Eq. (29) in the concept of LES. However, prior to this step the combustion system is typically reduced since the number of species and elementary reactions involved in combustion of hydrocarbon fuels is on the order of hundreds or thousands and it is far too large to solve with the presently available computational resources. In this thesis two different methods have been used, direct use of an ordinary differential equation (ODE) solver for finite rate chemistry in DNS and a heavily reduced system based on the levelset G-equation flamelet model for LES.

3.2.1 Finite Rate Chemistry

In DNS the resolution is fine enough so that all flow related and chemistry related time scales are resolved. However, when several species are involved in a combustion system the time scales of those reactions are usually very different, which results in a stiff system. During a relatively large CFD time step (which is typically set when using a low Mach number reacting flow solver) the mass fraction of intermediate species with short chemical time scales may vary substantially, which makes direct use of Arrhenius reaction rates induce large errors. Arrhenius rates are written for an elementary forward reaction $A + B \rightarrow C + D$:

$$-\frac{d[A]}{dt} = -\frac{d[B]}{dt} = \frac{d[C]}{dt} = \frac{d[D]}{dt} = [A][B]A_s T^{n_A} \exp(-E_a/\Re T), \quad (36)$$

where A_s, n_A, and E_a are reaction specific constants. An ODE solver for such a stiff system is therefore needed, which calculates the accumulated chemical reaction rates over the CFD time step through integration of multiple small time steps of adaptive size. In this thesis the chemistry mechanism by Li et al. [52] and the mechanism by Smooke and Giovangigli [11] were used for the H_2/air and the CH_4/air simulations respectively.

3.2.2 Levelset G-equation

The method described in section 3.2.1 is very demanding in terms of resolution and subsequently very computationally expensive. It is a challenge to apply finite rate chemistry in LES, since the reaction rates are computed based on filtered quantities and integrated over large CFD time steps ($\Delta t \sim$ μs). This direct use of finite rate chemistry in LES is generally not possible without case by case tuning of the chemical scheme and/or a well validated SGS model. An alternative approach is to replace the large number of species equations with either a reduced number of equations or equations that are representing the combustion process. The combustion model used in the LES studies in this thesis is the levelset G-equation [16], which is explained below.

3.2.2.1 Analytical Formulation

The main underlying assumption of using the levelset G-equation model is that the flame is of flamelet type and that the propagation of the flame can be described as the movement of an iso-surface. A propagation equation for such an iso-surface can thereafter be derived. By definition, the flame is characterized by the flame coordinate, G, through the equation:

$$G(\boldsymbol{x}, t) = 0. \tag{37}$$

Differentiation of this equation gives:

$$\frac{dG}{dt} = \frac{\partial G}{\partial t} + \frac{\partial G}{\partial x_j}\frac{\partial x_j}{\partial t} = 0, \tag{38}$$

where the term $\partial x_j/\partial t$, for a premixed flame, can be expressed through convection speed and self-propagation, S:

$$\frac{\partial x_j}{\partial t} = u_j + S \cdot n_j. \tag{39}$$

In Eq. (39), n_j is the j component of the flame front normal. The equation is solely valid at the iso-surface $G(\boldsymbol{x}, t)$ = 0; however, the G-field outside of the isosurface can be obtained by extending the G as a signed distance function. The flame front normal can then be expressed from the G-field:

$$n_j = -\frac{\partial G}{\partial x_j} \Big/ \left|\frac{\partial G}{\partial x_j}\right|. \tag{40}$$

Insert of Eqs. (39) and (40) in Eq. (38) results in the levelset G-equation:

$$\frac{\partial G}{\partial t} + u_j \frac{\partial G}{\partial x_j} = S \cdot \left|\frac{\partial G}{\partial x_j}\right|. \tag{41}$$

The extended G-field outside of the G = 0 iso-surface is defined by the signed closest normal distance to the flame. The sign is negative for the unburned gases and positive for the burned gases. This extension is called the reinitialization process and is performed through solving of the equation:

$$\left|\frac{\partial G}{\partial x_j}\right| = 1. \tag{42}$$

3.2.2.2 Filtered Formulation

When the G-equation model is employed within the LES and RANS frameworks the equation is solved for a filtered or averaged flame front instead of a fully resolved one. For LES, Eq. (41) is therefore expressed in terms of filtered G and u_j as:

$$\frac{\partial \tilde{G}}{\partial t} + \tilde{u}_j \frac{\partial \tilde{G}}{\partial x_j} = S_{LES} \cdot \left|\frac{\partial \tilde{G}}{\partial x_j}\right|, \tag{43}$$

where S_{LES} is the propagation speed of the filtered reaction zone. For closure of this equation, S_{LES} requires modeling. For the work conducted in this thesis, S_{LES} is expressed as:

$$S_{LES} = S_L \cdot \Xi_\Delta, \tag{44}$$

where Ξ_Δ is an SGS wrinkling factor accounting for unresolved flame wrinkling. By employing this expression it is assumed that the laminar flame speed is constant within one computational cell and that S_{LES} is directly proportional to the flame wrinkling, c.f. Eq. (9). Both S_L and Ξ_Δ therefore require modeling to be determined locally. In this thesis the

combustion model is applied to an atmospheric stratified premixed flame and S_L is therefore tabulated based on mixture fraction (Z) and strain (σ).

The majority of the models used for the SGS wrinkling factor can be summarized by the expression:

$$\Xi_\Delta = \left(1 + \alpha\left(\frac{u'_\Delta}{S_L + \beta}\right)^{n_c}\right)^{1/n_c}, \tag{45}$$

where α, β, and n_c are modeling parameters and u'_Δ is the SGS fluctuation, which requires estimation. Combining estimations of turbulent kinematic viscosity, ν_T, from the Smagorinsky model with the one from the RANS framework results in the SGS fluctuation estimation according to:

$$\begin{cases} \nu_T = (C_S\Delta)^2\sqrt{2\tilde{S}_{ij}\tilde{S}_{ij}} \\ \nu_T = C_\mu \cdot \Delta \cdot u'_\Delta \end{cases}$$
$$\Rightarrow$$
$$u'_\Delta = \frac{{C_S}^2}{C_\mu}\Delta\sqrt{2\tilde{S}_{ij}\tilde{S}_{ij}}. \tag{46}$$

In a previous work [53] the modeling parameters in Eq. (45) were assigned constant values: α = 3.1, β = 0.01 m/s, and n_c = 1, and adequate results were obtained. However, the constants in Eq. (46) are not uniquely defined and in this work a dynamic determination was therefore adapted.

The levelset G-equation combustion model for RANS and LES has been employed and validated for a wide range of combustion applications [22,23,53-56].

3.2.2.3 Dynamic Determination of the Wrinkling Factor

The constants for estimation of u'_Δ can be redefined as a single constant, $C = {C_S}^2/C_\mu$. The use of a set value for C is referred to as the static coefficient model (SCM). Test filtering (denoted by ^) on a scale larger than the LES grid, $\widehat{\Delta}$, results in:

$$\begin{cases} u'_{\Delta} = C\Delta\sqrt{2\tilde{S}_{ij}\tilde{S}_{ij}} \\ u'_{\widehat{\Delta}} = C\widehat{\Delta}\sqrt{2\hat{\tilde{S}}_{ij}\hat{\tilde{S}}_{ij}} \end{cases}. \tag{47}$$

$u'_{\widehat{\Delta}}$ can thereafter be estimated by,

$$\begin{aligned} u'_{\widehat{\Delta}} &= \sqrt{\frac{1}{3}\sum_i \widehat{\left(u_i - \hat{\tilde{u}}_i\right)^2}} = \\ &= \sqrt{\frac{1}{3}\sum_i \widehat{\left(\tilde{u}_i - \hat{\tilde{u}}_i\right)^2} + 2\widehat{\left(u_i - \hat{\tilde{u}}_i\right)}u'_{\Delta} + \widehat{u'^2_{\Delta}}} \approx \\ &\approx \left[\widehat{\left(\tilde{u}_i - \hat{\tilde{u}}_i\right)^2} \gg 2\widehat{\left(u_i - \hat{\tilde{u}}_i\right)}u'_{\Delta} + \widehat{u'^2_{\Delta}}\right] \approx \\ &\approx \sqrt{\frac{1}{3}\sum_i \widehat{\left(\tilde{u}_i - \hat{\tilde{u}}_i\right)^2}}. \end{aligned} \tag{48}$$

C can thereafter be simply determined through:

$$C = \sqrt{\frac{1}{3}\sum_i \widehat{\left(\tilde{u}_i - \hat{\tilde{u}}_i\right)^2}} \Big/ \widehat{\Delta}\sqrt{2\hat{\tilde{S}}_{ij}\hat{\tilde{S}}_{ij}}. \tag{49}$$

The use of Eq. (49) for dynamic determination of the SGS wrinkling factor is referred to as the dynamic coefficient model (DCM). DCM has been validated in Paper **V**.

3.2.2.4 Levelset G-equation in Stratified Premixed Combustion

The application of the levelset G-equation combustion model in this thesis is a lean premixed methane/air flame stabilized by a swirling flow and there are a few important physical phenomena that need to be captured by the combustion model in this case. First, the fuel/air mixture discharges from the burner into the surrounding air and can therefore be locally diluted prior to combustion. Second, as the equivalence ratio at the flame position decreases in the radial direction to zero in the ambient air, the flame will quench at some position. Third, after the flame the combustion products mix

with both cool ambient air and lean fuel/air mixture that has "leaked" past the flame.

In order to significantly reduce the number of species equations, but still capture these three physical phenomena, transport equations for the G-function, the mixture fraction, and the fuel species are employed. The G-function accounts for tracking of the flame, the mixture fraction accounts for mixing of products with unburned fuel and ambient air, and the fuel mass fraction accounts for mixing of the fuel-air mixture with ambient air prior to combustion as well as distinguishes between products and fuel that has leaked through quenched parts of the flame. The consumption of fuel is controlled through tabulation close to the $\tilde{G}$ = 0 levelset. The other species are following the G-function manifold and does not need to be solved for by transport equations individually.

3.3 Numerical Methods

3.3.1 DNS

Two different DNS codes have been employed, an open source code referred to as the pencil code (Paper **I**) and an in-house code (Papers **II** and **III**).

3.3.1.1 The In-house Code

The in-house DNS code [39] is of low Mach number type. The pressure is split in two parts, a thermodynamic pressure, $P(t)$, and a hydrodynamic pressure, $p_h(\boldsymbol{x}, t)$. The thermodynamic pressure, used in the equation of state, is constant in space whereas the smaller hydrodynamic pressure is the one used in the momentum equation. To be able to handle large density gradients the continuity equation is written in a material derivative form:

$$\frac{\partial u_i}{\partial x_i} = -\frac{1}{P}\frac{\partial P}{\partial t} + \frac{1}{T}\frac{DT}{Dt} + \sum_{k=1}^{N}\frac{\bar{W}}{W_k}\frac{DY_k}{Dt}, \tag{50}$$

with $\frac{D}{Dt} = \frac{\partial}{\partial t} + u_j\frac{\partial}{\partial x_j}$.

The in-house DNS code has been implemented in a vector form, which enables simple alternation between 1D, 2D, and 3D simulations. The code is

of finite difference type with a Cartesian grid structure. Temporal integrations of the convection-diffusion-reaction (CDR) terms in the governing equations are performed using an operator splitting technique. The 2nd order symmetrical Strang splitting algorithm [57] is employed where the stiff integration of chemistry is performed between two half-step integrations of the diffusion and convection terms. Integrations of the diffusion terms are however quite sensitive and needs to be further split into several sub-steps to satisfy the diffusion stability limit. In early studies (not included in this thesis), a 3rd order Runge-Kutta [58] temporal discretization was employed, but it was found during strict grid dependency tests that 2nd order Strang splitting showed a more desirable accuracy. The 3rd order Runge-Kutta scheme is however still used for the first time step of the simulations. Discretization of spatial terms in the governing equations is done through utilization of a 6th order central difference stencil except for the convective term in the species and energy equations. Due to large gradients of both species and temperature across the flame, these terms are discretized using a 5th order weighted essentially non-oscillating (WENO) scheme [59] to avoid unphysical oscillations close to such gradients. Especially in the species equations such oscillations can cause mass fractions to be negative or larger than unity. The detailed chemical kinetic mechanisms employed are integrated by a stiff solver, the double precision variable-coefficient ODE (DVODE) solver [60].

The use of the low Mach number assumption makes the CFD time step solely limited by maximum convection speed with associated Courant-Friedrichs-Lewy (CFL) condition and not by acoustic waves (speed of sound). However, due to the decoupling of the mass and the momentum equations, an equation to relate the velocity at time step $n+1$, u_j^{n+1}, with the velocity at the last fractional time step, u_j^*, and a pressure correction, p', is needed,

$$\frac{u_j^{n+1} - u_j^*}{\Delta t} = -\frac{1}{\rho^{n+1}} \frac{\partial p'}{\partial x_j}, \tag{51}$$

where ρ^{n+1} is the updated density at time step $n+1$. By taking the divergence of Eq. (51), a variable coefficient Poisson equation for the pressure correction is obtained:

$$-\frac{\partial}{\partial x_j}\left(\frac{1}{\rho^{n+1}}\frac{\partial}{\partial x_j}p'\right)=\frac{1}{\Delta t}\left(\frac{\partial}{\partial x_j}u_j^{n+1}-\frac{\partial}{\partial x_j}u_j^{*}\right). \quad (52)$$

The discretized continuity equation, Eq. (50), is used to replace $\partial u_j^{n+1}/\partial x_j$ with known quantities, P^{n+1}, T^{n+1}, and Y_s^{n+1} in Eq. (52). Equation (52) is discretized using 2nd order central difference, to avoid large discretization stencils, and solved implicitly using a multi-grid procedure. u_j^{n+1} is then obtained by solving Eq. (51) and the pressure is finally updated by:

$$p_h^{n+\frac{1}{2}}=p_h^{n-\frac{1}{2}}+p'. \quad (53)$$

Note that p_h is a lagged pressure defined on half time-steps to obtain second order accuracy for the discretized Eq. (51). Details on the multi-grid method can be found in [61,62] and further details on the discretization can be found in [39].

3.3.1.2 The Pencil Code

The pencil code is a high-order fully compressible DNS code available at a public domain [63]. Originally, the pencil code was developed for applications in astrophysics and magneto-hydrodynamics, but is applicable in combustion since a transport/chemistry module has been implemented [64]. Species diffusion coefficients and the heat conductivity are computed in a simplified way compared with the in-house code. Species diffusion coefficients are evaluated following [11]:

$$\rho D_s=\frac{D_0}{Le_s}\left(\frac{T}{T_0}\right)^{n_D}, \quad (54)$$

where D_0 is a mixture specific constant (D_0 = $2.58\cdot10^{-4}$ kg·m^{-1}·s^{-1} for CH_4/air mixture), T_0 is a reference temperature (T_0 = 298 K), and n_D = 0.7. The species Lewis numbers are assumed to be constant. Heat conductivity is computed through the expression [11]:

$$\lambda=D_0C_p\left(\frac{T}{T_0}\right)^{n_D}. \quad (55)$$

In the pencil code the equations are discretized using the 6th order central difference schemes for spatial derivatives on Cartesian grids. As mentioned in section 3.3.1.1 unphysical oscillations can occur due to high order central difference schemes and a 5th order upwind scheme was therefore used for convective terms in energy and species equations. For temporal discretization, an explicit 3rd order Runge-Kutta [58] scheme was used.

3.3.1.3 Turbulence Generation

In the DNS studies of flame/turbulence interaction, the turbulence fields were generated through a synthesizing method prior to the simulations. The turbulence fields were constructed based on pre-described turbulence spectra described by analytical functions [11,65]. These analytical functions were based on specified turbulent intensity and integral length scale [66-68]. A divergence free vector field is given by [66]:

$$\boldsymbol{u}(\boldsymbol{x}) = \sum_{s=1}^{S} \boldsymbol{v}(\boldsymbol{k}_s) \cdot cos(\boldsymbol{k}_s \cdot \boldsymbol{x}) + \boldsymbol{w}(\boldsymbol{k}_s) \cdot sin(\boldsymbol{k}_s \cdot \boldsymbol{x}), \qquad (56)$$

where $\boldsymbol{k}_s$ are wavenumber vectors. To assure a divergence free field, the directions of $\boldsymbol{v}$ and $\boldsymbol{w}$ are chosen to be perpendicular to $\boldsymbol{k}_s$, i.e.,

$$\boldsymbol{v}(\boldsymbol{k}_s) = C_F(\boldsymbol{k}_s) \cdot \boldsymbol{\zeta} \times \boldsymbol{k}_s, \;\; \boldsymbol{w}(\boldsymbol{k}_s) = C_F(\boldsymbol{k}_s) \cdot \boldsymbol{\xi} \times \boldsymbol{k}_s, \qquad (57)$$

where $\boldsymbol{\zeta}$ and $\boldsymbol{\xi}$ are arbitrary vectors picked from Gaussian distributions and C_F is a scaling factor. C_F is used to distribute the correct amount of turbulent kinetic energy between the different scales of turbulence, following the prescribed turbulence spectrum. C_F is given by:

$$C_F = \frac{8 \cdot E(\boldsymbol{k}_s)}{|\boldsymbol{\zeta} \times \boldsymbol{k}_s|^2 + |\boldsymbol{\xi} \times \boldsymbol{k}_s|^2}. \qquad (58)$$

In practice, the procedure is significantly speeded up by the use of fast Fourier transform (FFT).

In this thesis DNS of flame/turbulence interaction is employed in both 2D and 3D and for the 2D simulations some special considerations should be noted. 2D simulations lack the very important vortex stretching mechanism, which together with the reduction to two dimensions induce severe differences in the turbulence cascading between 3D and 2D turbulence fields. In several investigations [69-71] it has been shown that during flame/turbulence interaction, the interactions tend to appear at a higher extent with eddies of a cylindrical shape than spherical ones. Based on these observations one can expect that 2D simulations can be successfully used to reveal important physics (qualitatively). However, as the cascading is not physically correct, quantitative conclusions are not possible to draw and trends that are found in 2D must be verified by 3D simulations.

3.3.2 LES

Large eddy simulations were performed using a finite difference in-house solver (Papers **IV-VI**). The code utilizes staggered Cartesian grids for discretization of the filtered governing equations. For speeding up convergence, the code is using a multi-grid structure [72].

The convective term in the momentum equation is discretized using a 3rd order upwind scheme [73]. Due to the odd order discretization, the concept of ILES can be employed with no explicit SGS model as described in section 3.1.3.2. Other spatial derivatives in equations (25, 26) and the scalar equations are discretized using a 4th order central difference scheme. Time integration is computed using a 2nd order implicit scheme. The G-equation requires a bit different treatment due to its correlation with high density gradients and a more stable discretization needs to be employed. Spatial derivatives are computed through a 3rd order WENO scheme [59] and the time integration is performed using a 3rd order Runge-Kutta total variation diminishing (TVD) scheme [58].

3.4 Dynamic Mode Decomposition (DMD)

For determination of spatial structures characterized by frequencies and rate of growth or decay from a given set of data (numerical or experimental), dynamic mode decomposition (DMD) [74,75] has been recently developed. The approach used in this thesis will be shortly presented here. A set of (column) data is provided $\{u_k\}_{k=1}^{m}$. This can be several time sequences for a

point measurement or ≥ 1D measurements at several time instances. The last set of data (m) is replaced by a linear combination of the previous datasets:

$$u_m = \sum_{k=1}^{m-1} c_k u_k, \tag{59}$$

where the weight coefficients c_k are computed through least square fitting. The columns are combined to a matrix U:

$$U = [u_1\ u_2\ \dots u_m]. \tag{60}$$

If it is assumed that one set of data can be given by the previous through applying an operator A ($u_{k+1} = Au_k$), the expression:

$$AU = UC \tag{61}$$

is valid for the companion matrix C:

$$C = \begin{bmatrix} 0 & & & & c_1 \\ 1 & 0 & & & c_2 \\ & \ddots & \ddots & & \vdots \\ & & 1 & 0 & c_{m-2} \\ & & & 1 & c_{m-1} \end{bmatrix}. \tag{62}$$

From the companion matrix, an eigenvalue problem is stated:

$$Cx = \sigma_e x, \tag{63}$$

from which eigenvectors (dynamic modes) and eigenvalues, σ_e, are solved for. The eigenvalues are related to λ_e through $\sigma_e = e^{\lambda_e \cdot t}$. The real and the imaginary parts of λ_e correspond to the growth/decay rate of the mode and the oscillating frequency of the mode, respectively.

Chapter 4
DNS of Distributed Combustion

In this chapter fundamental studies of turbulent premixed combustion utilizing direct numerical simulations are summarized. The results shown here are primarily based on the simulations presented in Papers **II** and **III** and unpublished CH_4/air simulations. Detailed results are given in Papers **I-III**.

4.1 Flame Structure

As previously mentioned in Chapter 2, the broken or distributed reaction zone regime is defined by Peters as the regime with the Karlovitz number larger than 100 [16]. This definition is based on phenomenological and asymptotic arguments that with Karlovitz number lower than 100 the inner flame structure is left unperturbed, which modelers have widely used for justification of the use of flamelet models in the thin reaction zone regime. However, few studies of flame-turbulence interaction in or around the Ka = 100 boundary have been conducted and whether this boundary is actually correct or not has not been brought to a general consensus.

The studies in Paper **I** are based on 2D simulations of CH_4/air flames at high Karlovitz numbers. In this paper it was reported that broadening of the inner layer of the reaction zone was not observed for Karlovitz numbers below 2000, whereas broadening was observed for the Ka = 9500 case. Regarding these simulations a few important notes should be made. First, during the simulation times the turbulence fields experienced a significant decay of turbulent intensity since no turbulence forcing was employed. Second, as the computational domain was 2D the turbulent energy cascading from large to small scales was not physically correct, which rather than feeding energy to the small scales enhances vortex pairing and maintains the energy on large scales. Third, transport coefficients and chemical reaction rates were computed based on a simplified approach, diffusion coefficients were obtained through Eqs. (54) and (55) and chemical source terms through direct use of Arrhenius rates. Since the simulation code (the Pencil Code) is fully compressible and the CFD time step is limited by the speed of sound, the accuracy of direct use of Arrhenius rate is likely acceptable. However, as shown in Papers **II** and **III**, the physics in distributed flames is highly sensitive to detailed transport and the

simplified transport through Eqs. (54) and (55) should be brought in mind. These initial 2D studies can therefore be considered for qualitative analysis, but to deduce quantitative conclusions 3D simulations with detailed transport and a stiff ODE solver are necessary.

In Papers **II** and **III** the second and third considerations mentioned above were taken into account and 3D simulations employing a stiff ODE solver for the detailed chemistry were performed. Turbulence forcing was not employed; however, as the considered time interval was very short, the flames were maintained in the distributed reaction zone regime throughout

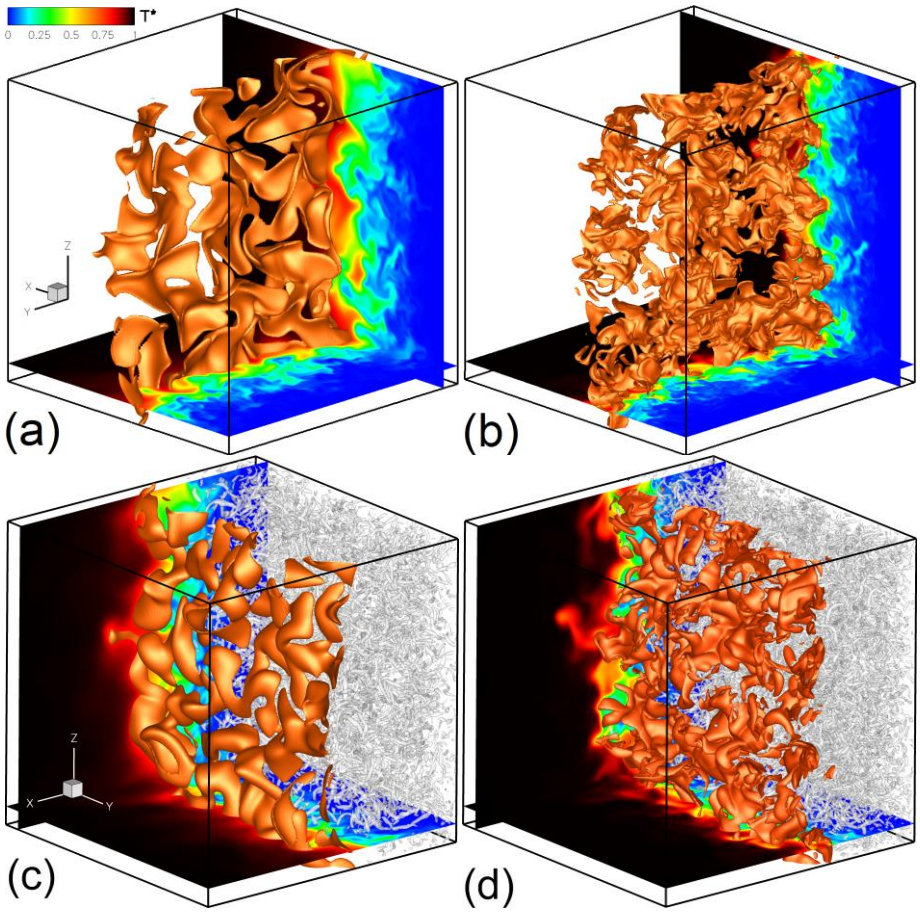

Figure 4.1. Front and back views of instantaneous snapshots of 3D high Karlovitz number flames for a CH_4/air flame (a) and (c), and H_2/air flame (b) and (d) at t/τ_l = 1.25. Flow turbulence is visualized using λ_2 isosurfaces (grey); the reacting front (orange) is defined at the iso-surfaces of HRR* = 1.2. Temperature contours are shown on the 2D slices.

the simulations. Figure 4.1 shows the front and back views of the normalized heat release rate (HRR*), the isosurfaces of λ_2, and temperature for CH_4/air and H_2/air flames at an initial Karlovitz number of 1860. The peak heat release rate in a 1D flame is used for normalization of the heat release rates. A significant difference between the two flames is notable. The H_2/air flame appears more distributed than the CH_4/air flame, which can be attributed to a smaller Kolmogorov length scale and differential diffusion effects. This discrepancy will be discussed in further details in Section 4.2.2.

In unpublished simulations, premixed CH_4/air flames for a range of Karlovitz numbers ($125 \leq Ka \leq 3350$) have been studied. Figure 4.2 shows temperature and HRR* fields from developed flames of Ka = 125, 550, 900, and 3350. In these simulations a low wavenumber forcing method has been used for the unburned gases, which allows the turbulence to be maintained throughout the simulations. From Fig. 4.2 it can be noted that as the Karlovitz number increases, small scale turbulence interaction with the flame becomes intensified. The temperature zone becomes more spread at higher Karlovitz numbers and the HRR* layer becomes locally thinner and thicker compared with the lower Karlovitz number flames.

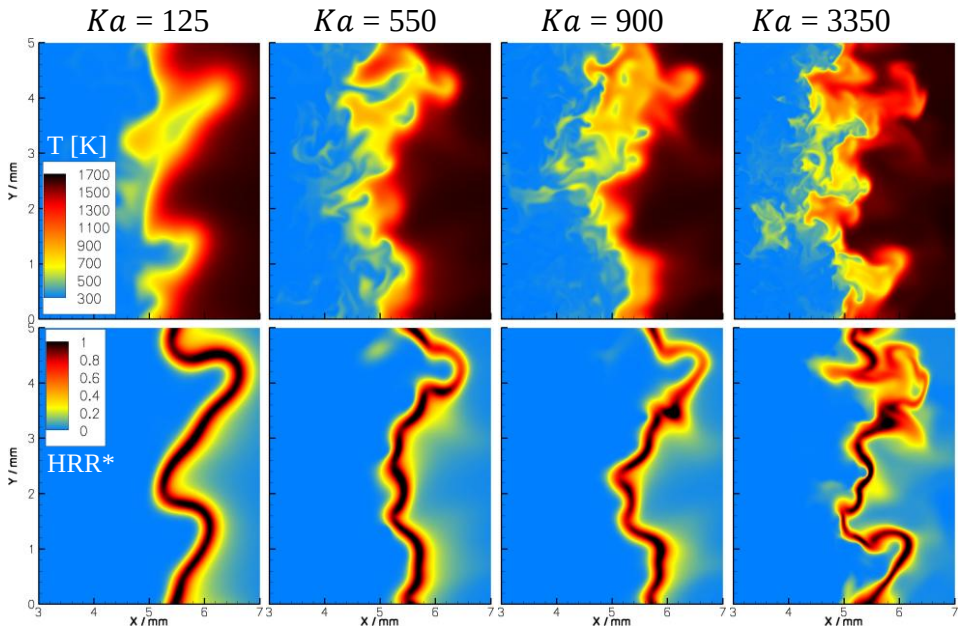

Figure 4.2. Temperature and normalized heat release rate for turbulent lean CH_4/air flames at Karlovitz numbers of 125, 550, 900, and 3350.

4.2 Detailed Chemistry Effects

4.2.1 Turbulence Induced Change of Chemical Pathway

When intense small scale turbulence interacts with the detailed chemistry layers of a flame, combined convective-diffusive transport can make the mapping of Y_s in T-space non-unique. As an example of such mixing, joint probability density functions (JPDFs) of T with Y_{H} and $Y_{\mathrm{HO_2}}$ for a CH_4/air flame and an H_2/air flame, both at Ka = 1860, are shown in Fig. 4.3. It can be seen in Fig 4.3 that high turbulent intensities give rise to a significantly increased concentration of these intermediate species in the low temperature zone. An increased species concentration is either due to transport or reaction, therefore, in order to determine the origin of these increased species concentrations, one must investigate the corresponding reaction rates. Figure 4.4 shows JPDFs of T with HRR*, $\dot{\omega}_{\mathrm{H}}/\rho$, and $\dot{\omega}_{\mathrm{HO_2}}/\rho$. It can be noted from Fig. 4.4 that $\dot{\omega}_{\mathrm{H}}/\rho$ is largely negative at low temperatures. This implies that the increased concentration of H at low temperature is not due to formation, but due to convective-diffusive transport from the high temperature zone to the low temperature zone. $\dot{\omega}_{\mathrm{HO_2}}/\rho$ on the other hand is largely positive at low temperatures, which implies that the increased concentration of HO_2 at low temperatures is due to an increased formation

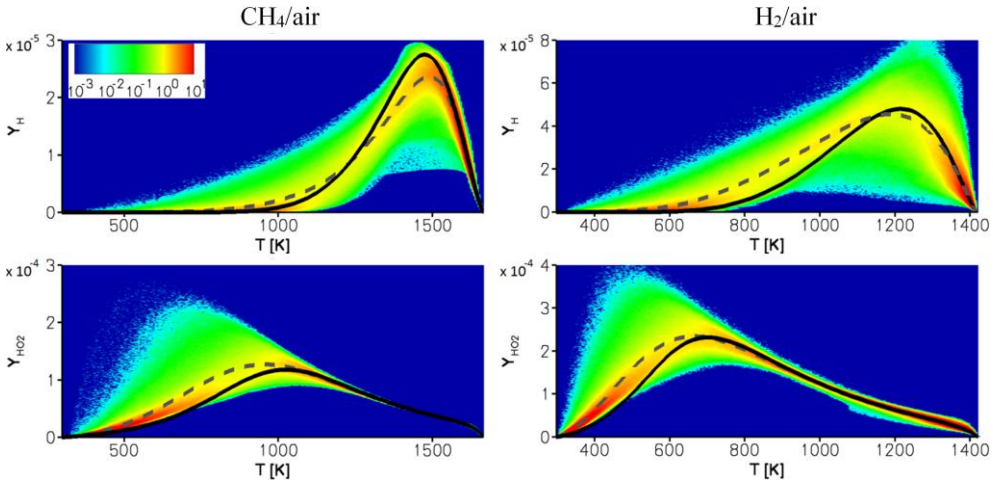

Figure 4.3. JPDFs of T with Y_{H} and $Y_{\mathrm{HO_2}}$ for a CH_4/air flame and an H_2/air flame at Ka = 1860. Solid lines denote distributions in 1D flames and dashed lines are averages conditioned on T.

of HO_2 in that region. The local values of Y_{HO_2} in the low temperature range are larger than the peak values in the 1D flames and convective-diffusive transport is therefore not the dominating contributor. In Fig. 4.4 it can also be seen that the heat release rate in the low temperature zone is significantly increased for these high Karlovitz number cases compared with the laminar or the low Karlovitz number flames. It turned out that the three different reaction rates shown in Fig. 4.4 are all related through the three body recombination reaction $H+O_2+M \rightarrow HO_2+M$. The convective-diffusive transport of H radicals from the high temperature zone to the low temperature zone significantly increases the rate of this elementary reaction at low temperatures and makes it responsible for the large consumption of H radicals, large formation of HO_2, and the significant heat release rate at low temperatures. The three body recombination reaction is exothermic and as it turns out, can contribute to a significant heat release rate at low temperatures in a high Karlovitz number flame.

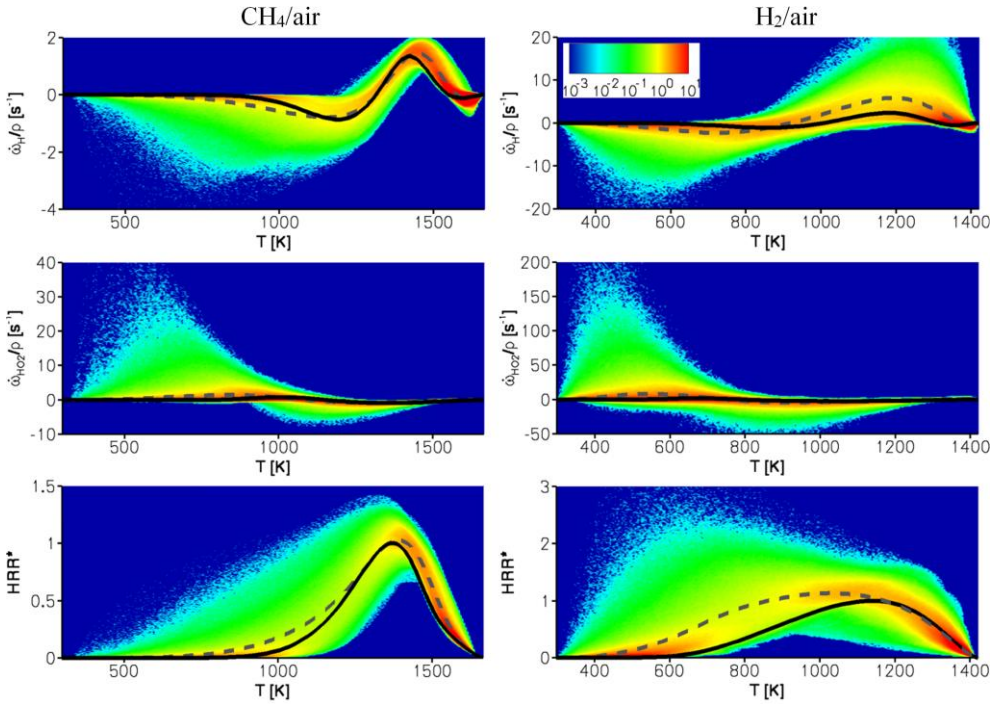

Figure 4.4. JPDFs of T with $\dot{\omega}_H/\rho$ and $\dot{\omega}_{HO_2}/\rho$ for a CH_4/air flame and an H_2/air flame at Ka = 1860. Solid lines denote distributions in 1D flames and dashed lines are averages conditioned on T.

The reaction rate of the three body recombination reaction is dependent on (and influences), besides H radical concentration and temperature, the oxygen concentration. Since the studied flames are both lean premixed flames, the variation of oxygen concentration at low temperatures can be expected to be low and does not strongly influence the reaction rate of this elementary reaction. However, if the global reaction rate of the oxygen species is investigated, shown in Fig. 4.5 for the two different flames, one can see that the oxygen consumption at low temperatures is significantly increased. Also notable from the inset in Fig. 4.5 is the positive oxygen reaction rates found in the H_2/air flame. These positive global reaction rates are also a consequence of the intensified elementary reaction rate of the three body recombination reaction. As the increased concentration of HO_2 reacts towards products at equilibrium ($H_2O+O_2+N_2$), local compositions can give rise to positive global reaction rates of the O_2 species. These changes in species reaction rates and heat release rates in the low temperature range for high Karlovitz number flames can be summarized as a significant change in chemical pathway from the one of 1D or low Karlovitz number flames.

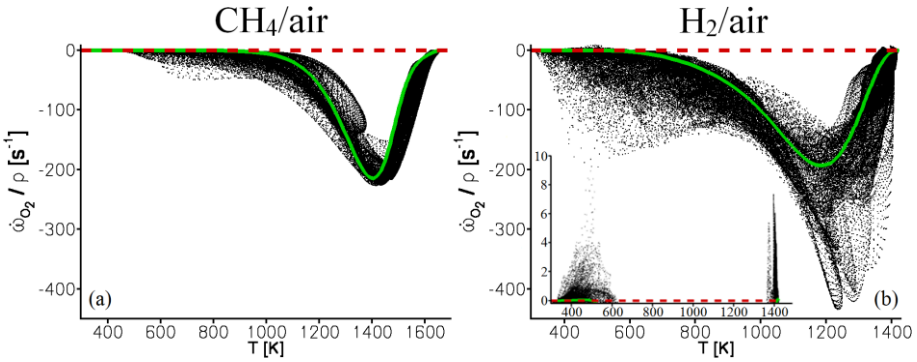

Figure 4.5. Scatter plots of $\dot{\omega}_{O_2}/\rho$ vs. temperature at t/τ = 1.25 from the CH_4/air flame (left) and the H_2/air flame (right) at t/τ = 1.25. Solid lines correspond to the 1D laminar flame solutions. Dashed lines denote $\dot{\omega}_{O_2}/\rho$ = 0 s^{-1}.

4.2.2 Characterization of Distributed Flames

In addition to the detailed chemistry effects in high Karlovitz number flames mentioned above, it should also be noted from Figs. 4.1, 4.4, and 4.5 that the H_2/air flame appears, both visually and statistically, more distributed than the CH_4/air flame. The Karlovitz numbers of the two flames are identical

(Ka = 1860); however, especially in terms of the detailed chemistry effects on the flame structure, significant differences between the two flames can be noted. To account for these differences in the classification of turbulent premixed flames, a species specific Karlovitz number, Ka_s, is proposed,

$$Ka_s = \tau_s^L / \tau_\eta. \tag{64}$$

In Eq. (64) τ_s^L is a chemical time scale for individual species s, which is calculated from a steady 1D laminar flame solution as:

$$\tau_s^L = \int_0^1 Y_s dc \Big/ \int_0^1 \left|\frac{\dot{\omega}_s}{2\rho}\right| dc. \tag{65}$$

The factor 2 in the denominator of Eq. (65) is introduced to account for the cancelation of positive production rates and negative consumption rate for any intermediate species s in a steady flame solution. When defining a new characterization it is important to not introduce inconsistencies with previous definitions. In these cases, for the CH_4/air flame, $\tau_{CH_4}^L$ = 8800 μs and for the H_2/air flame, $\tau_{H_2}^L$ = 3100 μs. These (fuel based) time scales are similar to $\tau_c = \delta_L / S_L$ for the two flames, respectively. The definition of Ka_s is therefore consistent with Ka.

Figure 4.6 shows the temporal evolution of an effective Karlovitz number (Ka_{eff}), the turbulent intensity, and species specific Karlovitz numbers of H and HO_2 during two integral time scales. The turbulent intensity and integral length scale are at each time instance computed for the unburned gases and the effective Karlovitz number (based on Eq. 11) and the species specific Karlovitz number are both based on these quantities. It can be seen in Fig. 4.6 that the effective Karlovitz numbers of the two flames evolve similar in time and maintain comparable magnitude throughout the simulations. From the species specific Karlovitz numbers there are two things worth noting. First, the Karlovitz numbers based on HO_2 are roughly one order of magnitude larger than the Karlovitz numbers based on H. This corresponds well to the differences in the radical layers structure (see Fig. 4 in Paper **III**). Second, the species specific Karlovitz numbers are higher for the H_2/air flame compared with the CH_4/air flame. This in turn corresponds well to the difference in the radical layers between the two flames (see Fig. 4 in Paper **III**). The species specific Karlovitz number is therefore able to

better account for the effect of turbulence scales on the inner radical layers of the flame compared with the conventional Karlovitz number.

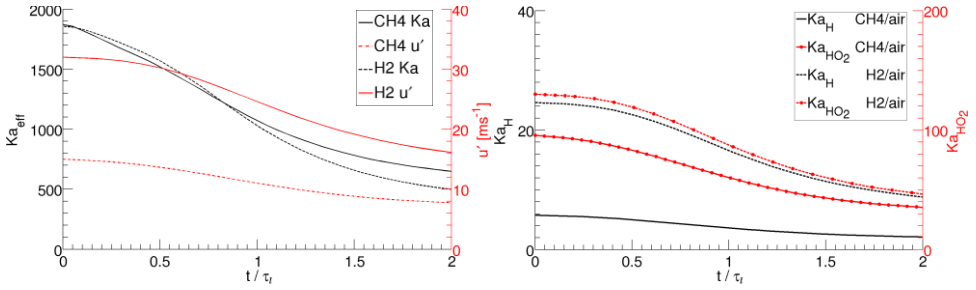

Figure 4.6. Evolution of the effective Karlovitz number, the turbulent intensity, and the species specific Karlovitz number of H and HO_2 during two integral time scales.

As for the conventional Karlovitz number, the species specific Karlovitz number is based on a phenomenological argument with an estimated Kolmogorov time scale in the definition. In order to investigate the true effect of turbulence on the inner layers of the flame, additional analysis needs to be conducted. Since the setup of the present flame configuration is a channel flow type with periodic spanwise and lateral boundaries, the flame structure can be straightforwardly studied with the Fourier transform by assuming statistically homogeneity and isotropy in the spanwise-lateral plane. A two-point correlation function in a chosen y-z plane for variable $\psi(\boldsymbol{x})$ is defined as: $R_\psi(\boldsymbol{r}) = \langle\psi(\boldsymbol{x}+\boldsymbol{r})\psi(\boldsymbol{x})\rangle_{yz}$, where $\boldsymbol{r}$ represents a vector in the y-z plane. $\langle\cdot\rangle_{yz}$ denotes averaging in the y and z directions. $\hat{R}_\psi$ is then obtained by applying the 2D Fourier transform $\mathcal{F}$ to R_ψ: $\hat{R}_\psi(\boldsymbol{\kappa}) = \mathcal{F}\left[R_\psi(\boldsymbol{r})\right]$, where $\boldsymbol{\kappa}$ is a 2D wavenumber vector. A 1D power spectral density spectrum, $E_\psi(\kappa)$, can be computed as:

$$E_\psi(\kappa) = \frac{1}{2\pi\cdot\kappa}\iint \hat{R}_\psi(\boldsymbol{\kappa})\,\delta(|\boldsymbol{\kappa}|-\kappa)d\boldsymbol{\kappa}, \tag{66}$$

where $\delta(\kappa)$ is the Dirac delta function. E_ψ can be integrated for the entire 1D spectrum to give an estimation of the ψ fluctuation level, containing a correlation length scale. For a species s, similar to that in a laminar flame (cf. Eq. 65), the characteristic chemical time scales in high Karlovitz number flames depend on both the distribution of species s and the chemical

rate of species s. Since the reaction zones are highly distorted in high Ka flames, chemical reactions involving a given species s occur at a wide range of spectrum of length and time scales. To take this into account a turbulent effective chemical time scale of species s, τ_s^T, is defined as:

$$\tau_s^T = \left(\int E_{Y_s}(k)dk \Big/ \int E_{\dot{\omega}_s/\rho}(k)dk \right)^{1/2}. \tag{67}$$

Note, the above defined τ_s^T can vary with both x and t, which can be mapped to the $\langle c \rangle_{yz}$ space. A non-dimensional ratio $\bar{\alpha}_s$ comparing the laminar and the turbulent time scales of species s is defined as:

$$\bar{\alpha}_s = \tau_s^L \Big/ \int_0^1 \tau_s^T dc. \tag{68}$$

Figure 4.7 shows Ka_s and $\bar{\alpha}_s$ for species H and HO_2 during two integral time scales for the CH_4/air flame. At the initial stage $\bar{\alpha}_s$ is zero due to an initially unperturbed planar flame front. With an increasing flame-turbulence interaction, $\bar{\alpha}_s$ is increasing until it reaches a maximum where the turbulence decay makes the turbulence unable to induce further wrinkle and in-flame distribution of the flame front. After this peak (which occur at roughly t/τ_l = 1) $\bar{\alpha}_{HO_2}$ decays similar as Ka_{HO_2}. From Fig. 4.7 it can be seen that $\bar{\alpha}_{HO_2}$ and Ka_{HO_2} collapse for the developed flame brush ($t/\tau_l \gtrsim 1$), whereas $\bar{\alpha}_H$ is larger than Ka_H but in the same order of magnitude. The discrepancy between $\bar{\alpha}_H$ and Ka_H can be either due to physically different interaction between the small scale turbulence and the H radical layer compared with the one for HO_2 and the one estimated through Ka_H or due

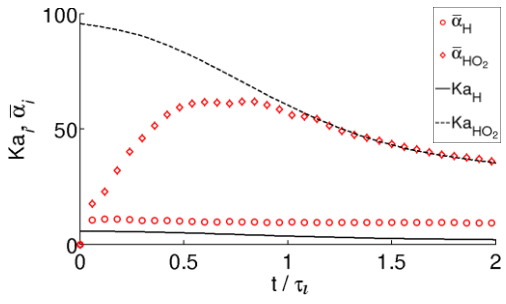

Figure 4.7. Ka_s and $\bar{\alpha}_s$ for species H and HO_2 during two integral time scales.

to minor inconsistencies in the definitions between $\bar{\alpha}_i$ and Ka_i. In order to delineate the underlying reason, further validation studies are required.

Chapter 5
LES of Low Swirl Stabilized Flames

In this chapter the more applied approach (compared with DNS) of LES using a flamelet model is presented, where the combustion model is evaluated for a swirl flame case. Detailed results are given in Papers **IV-VI**.

5.1 The Low Swirl Burner

When evaluating a model one needs to take into account a couple of important considerations. First, and most important, for the considered test case, sufficient validation data should be available. This data can be either experimental or from a DNS database, but the accuracy of the validation data should be carefully considered. Second, since all models are developed based on some assumptions, the test case should not conflict with these assumptions. Third, additional uncertainties that are associated with the choice of test case should be minimized, e.g., unknown boundary conditions etc. A suitable case that meets these requirements for LES is the low swirl burner experimental rig [8,76] that has been the target of extensive experimental and numerical campaigns at Lund University (LU) and Lawrence Berkeley National Lab (LBL) during the past two decades [53,76-81]. From these previous studies an extensive validation data base is available where it has been shown (amongst other things) that the flame behaves like a flamelet and is therefore suitable to the modeling assumptions. Moreover, as the flame is swirl stabilized at a rather significant distance from the burner, modeling of reactions close to walls is avoided, which simplifies the boundary conditions.

The low swirl burner was first developed at LBL, but the burner design that has been used at LBL and LU during the past decade has a modified swirl arrangement. Figure 5.1a and b show front and side views of the burner geometry, where the swirler design can be seen. The fuel/air mixture passes through either a central perforated plate (where no swirl is generated) or an annular swirler. The central plate has 37 holes, each with a diameter of 3.6 mm and the diameter of the perforated plate is 39.6 mm. The swirler has eight guide vanes which has an exit angle of 37 degrees in relation to the vertical axis. The swirling mixture exits through a nozzle (diameter D = 50 mm) into a wide low speed co-flow of air, which shields the measurement zone from dust-particles. The mass flow split between the perforated plate

and the swirler results in rather different characteristic velocities for different flow regions. Figure 5.1c shows a schematic view of the central cross section of the burner. The characteristic velocities are $v_1 \sim 5.6 \cdot 10^{-4} \cdot Re$ m/s, $v_2 \sim 2.4 \cdot 10^{-4} \cdot Re$ m/s, and $v_3 \sim 0.35$ m/s. Re is based on the burner diameter and the mean bulk flow velocity. At low Reynolds numbers (read <30,000), as the flow is not self-similar, the mass flow split and thereby the characteristic velocities are a bit different. The differences in velocities between v_1 and v_2, and v_1 and v_3 result in an inner and an outer shear layer, respectively, which are also marked schematically in Fig. 5.1c.

Similar setups of the burner have also been utilized in separate studies [82-85].

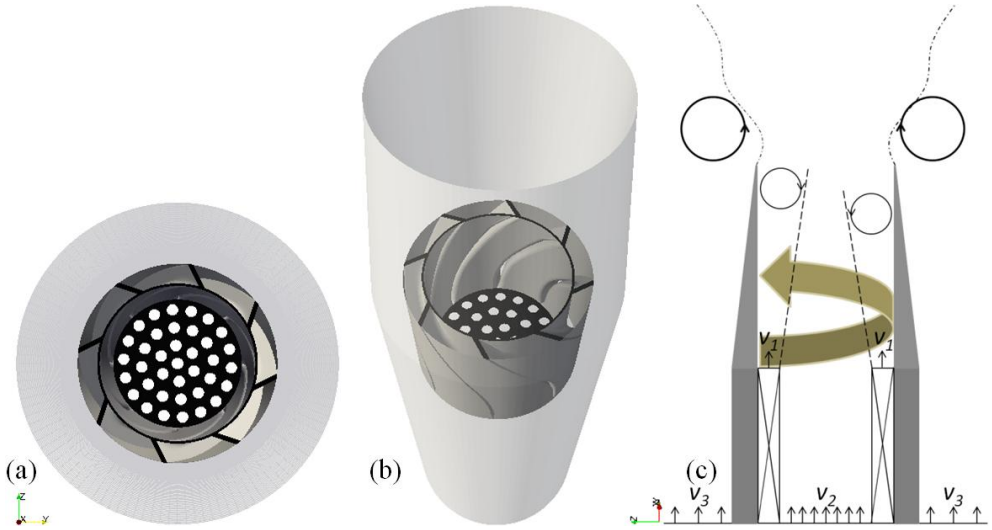

Figure 5.1. Front (a) and side (b) views of the burner geometry and a schematic drawing of the burner induced flow field (c).

5.2 G-equation Modeling Validation

5.2.1 Previous Validation

The use of the levelset G-equation combustion model for LES has been validated for low Reynolds number flows in the low swirl burner in previous studies [53,77]. These validation campaigns were focused on a proper modeling of the leading flame region and the flow field upstream of the leading flame. It was concluded that a modeled boundary condition

through set of a mean velocity field (from experiments) and modeled turbulent fluctuations at the nozzle exit plane could not account for the real turbulent structures and subsequent dynamics of the flame and the flame was blowing off. If the flow field inside the burner geometry instead was simulated with LES, flame stabilization was achieved. Based on these conclusions, the flow fields inside the burner were simulated with LES for the different investigated Reynolds numbers and the velocity fields at the nozzle exit plane was sampled from iso-thermal flow simulations and imposed as inflow boundary conditions for the reacting flow simulations.

Due to limited experimental support in the downstream regions, where the combustion products are cooled by entrainment of ambient air, the model performance in such conditions was not evaluated in the previous works. The behavior of the temperature field in the downstream regions is influenced by some different factors, e.g., inflow turbulence, flame quenching/re-ignition, and radiation heat loss, and different LES with different combustion models showed significant diversity in the behavior in this region. It is therefore of essential importance to have access to temperature measurements in the cooling/entrainment region of the flame for validation of the models.

5.2.2 Present Validation

In the initial stages of this project a new series of combined temperature and O_2-mole fraction measurements in the low swirl burner flame were performed at LU. The measurements were performed using rotational coherent anti-Stokes Raman spectroscopy (RCARS), which is a point measurement technique, and through ca 1000 measurements at ca 130 positions rather complete temperature and O_2-mole fraction fields at a 2D cross-section plane were obtained. The measurements were performed for a CH_4/air mixture of ϕ = 0.62 and Reynolds numbers of 20,000 and 30,000. In Paper **IV** measurements along the center axis of the burner at Re = 20,000 were presented along with G-equation LES results using SCM for the SGS wrinkling factor (see Section 3.2.2.3). In this paper it was shown that the flame position, the dynamic motion of the leading edge of the flame, and the entrainment rate of cooling ambient air to the combustion products were reasonably captured by the LES model. However, as it was shown in previous work that the flame was sensitive to the inflow boundary condition [53], new studies of the burner flow needed to be conducted. In Refs. [53,78] and Paper **IV** the inflows were simulated with a resolved swirler and

a modeled perforated plate and to improve the quality of the inflow boundary condition new swirler flow simulations were conducted. In the new simulations both the swirler and the perforated plate were resolved with a finer mesh. These iso-thermal simulations were performed for Reynolds numbers of 20,000, 25,000, 30,000, 50,000, and 100,000, where the Reynolds numbers of 20,000 and 30,000 were used as inflow boundary conditions in the reacting flow solver (experimental cases). In the first simulations of the low swirl flame with LES SCM using the new inflow boundary condition, it was found that the mean flame position and the dynamic fluctuations of the flame were very well captured; however, the entrainment rate of cooling air at the downstream positions were under-predicted. The entrainment of ambient cooling air at downstream positions is closely linked with the dynamic motion of the flame in the shear layer region, where the entrained gases origin. To better capture this effect, the dynamic formulation of the wrinkling factor (see Section 3.2.2.3) LES DCM was implemented. Figure 5.2 shows time averaged mean and root-mean-square (rms) of temperature from LES SCM, LES DCM, and RCARS along the center axis of the burner for the Re = 30,000 case. It can be seen in Fig. 5.2 that the rate of entrainment of ambient air to the center axis is better captured with the LES DCM compared with the LES SCM. The locally dependent wrinkling factor makes the propagation speed of the filtered reaction front more sensitive to variations in the flow field, especially in the shear layer region, and enables a more rapid entrainment of cooling air to the product gases.

It is important for a good model to be functional in a wide range of operating conditions. The low swirl flame is also a suitable case for this type of validation. Previous work has shown strong sensitivity of the case to Reynolds number [78,79] and the new RCARS measurements were

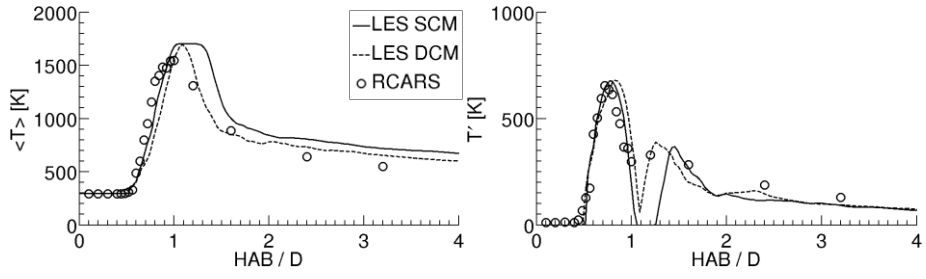

Figure 5.2. Time averaged mean and rms of temperature along the center axis of the burner; comparison between LES SCM, LES DCM, and RCARS.

performed to create 2D mappings for two different Reynolds numbers of 20,000 and 30,000. Figure 5.3 shows iso-lines of different time averaged mean and rms temperatures from LES DCM and RCARS for the Re = 20,000 and 30,000 cases. Figure 5.3 clearly shows that the LES DCM model is very well capturing the Re dependency of the flame with a more rapid entrainment of cooling ambient gases in the downstream regions at increasing Reynolds numbers. For both Reynolds numbers both the mean and the fluctuations of the leading edge of the flame as well as the air entrained region are in close agreement between simulations and experiments.

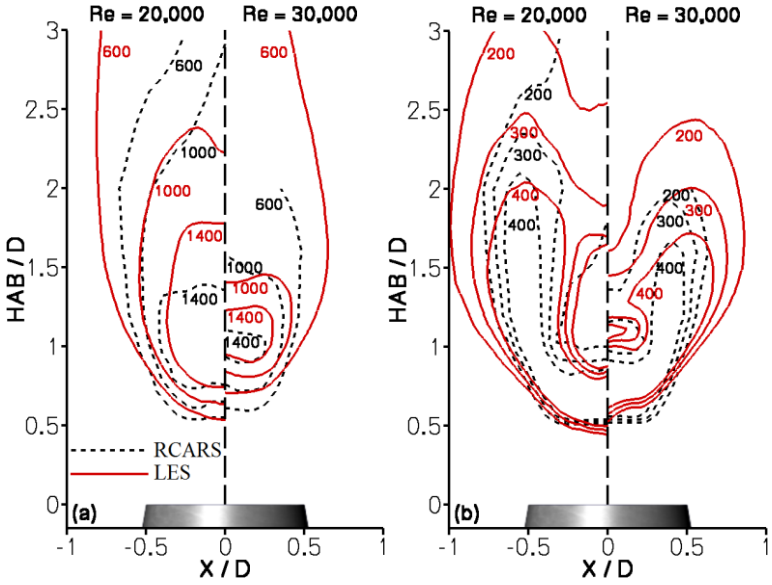

Figure 5.3. Time averaged mean (a) and rms (b) temperature from LES (solid lines) and RCARS (dashed lines) for the Re = 20,000 and 30,000 cases.

5.3 Low Swirl Flame Dynamics

It is evident from section 5.2 that the G-equation model is able to capture key characteristics of the low swirl flame in terms of the mean and the rms of temperature. The model can therefore be rather confidently used to study other features of the flame. It is well known that swirl stabilized flames exhibits dynamics of low frequency large scale coherent structures. Recent numerical and experimental studies [78,80] have also shown that this is the

case for the low swirl flame. In Paper **VI** studies of the effect of such large scale structures on the motion of the flame have therefore been conducted.

From Ref. [78] it is known that shear layer instabilities in and above the burner nozzle generates strong frequency signals which are suspected to be linked to large scale coherent structures. In Paper **VI** it is shown that by the use of dynamic mode decomposition (DMD) the two frequencies obtained in Ref. [78] are connected to two clear coherent frequency specific flow structures that origin from the inner and outer shear layers of the burner flow, respectively. In order to directly couple the effect of these flow structures to the motion of the flame an extended DMD was performed for the flow variables ($\boldsymbol{u}$) together with a flame variable (the G-function). Figure 5.4 shows the 3D structures of the real and imaginary parts of the outer shear layer mode I and the inner shear layer mode II, which are corresponding to frequencies of 175 Hz and 211 Hz, respectively. Orange and white iso-surfaces represent the radial velocity component of the modes and blue and red iso-surfaces represent the flame surface component of the mode (the G-component). To clarify the coherent structures of modes I and

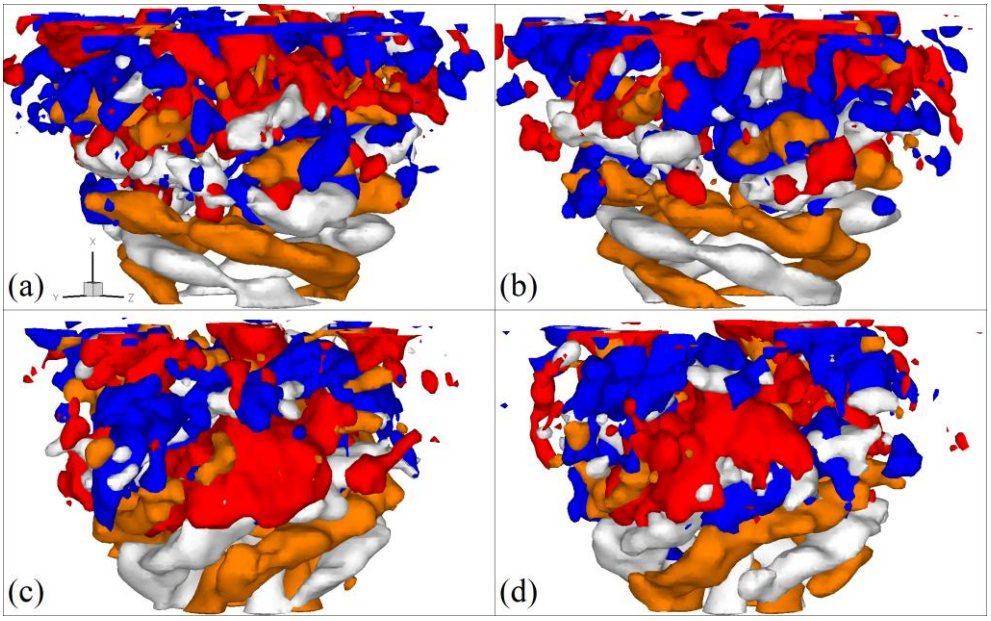

Figure 5.4. Real and imaginary parts of LES DMD modes I, (a) and (b), and II, (c) and (d). The modes are visualized through iso-surfaces of positive and negative radial velocity, orange and white surfaces respectively, and iso-surfaces of positive and negative G-field values, red and blue surfaces respectively.

II, horizontal cross sections of the radial velocity component at height above burner (HAB) = 15 mm and G-component at HAB = 35 mm are shown in Fig. 5.5. From Figs. 5.4 and 5.5 it clear that even though the coherent structures of the flow are evident for both modes, the effect of the different flow structures on the flame appears quite different. Mode I, which is the mode with origin in the outer shear layer, shows no clear correlation between flow and flame structures. This is consistent with previous studies [78,80], where it was proposed that it is the vorticity generated by the inner shear layer that is contributing to flame stabilization whereas the outer shear layer generated vorticity is simply convecting the flame downstream.

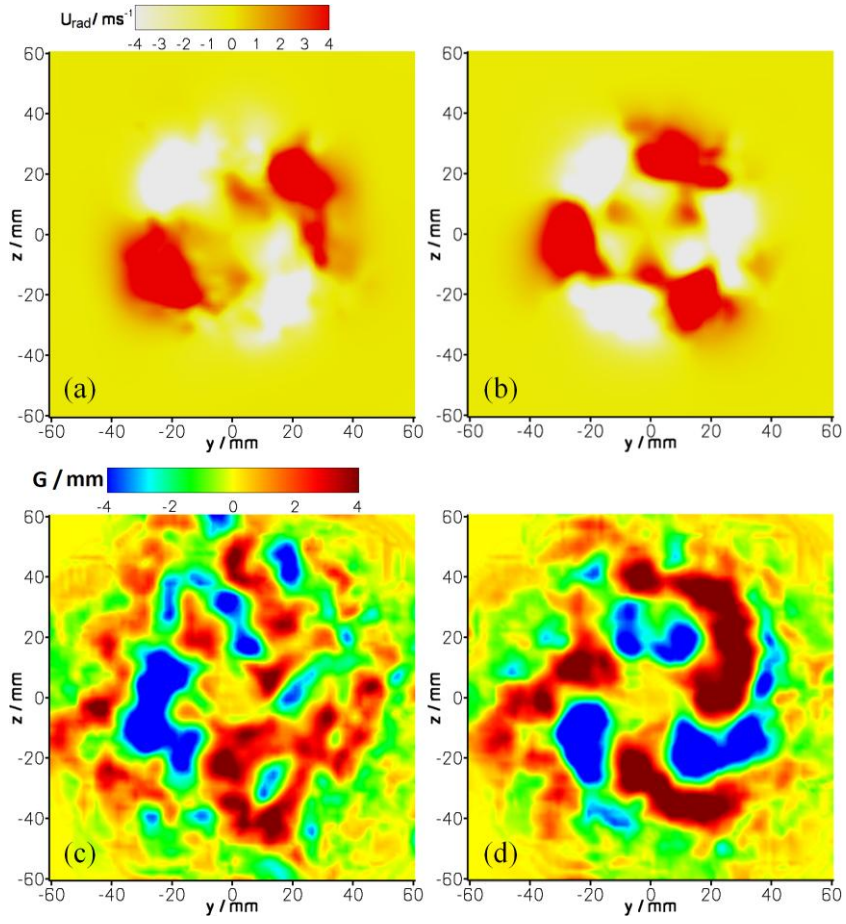

Figure 5.5. Horizontal cross-sections of the real part of mode I and II of the radial velocity at HAB = 15 mm, a and b respectively, as well as horizontal cross-sections of the real part of mode I and II of G at HAB = 35 mm, c and d respectively.

Furthermore, also consistent with these previous studies is that mode II shows a clear correlation between the motion of the frequency specific flow structures and the flame motion. The three-armed motion of the velocity field of the mode is directly followed by a three-armed motion of the flame. Mode II has its origin in the inner shear layer and by further superimposing the mode onto the mean G-field the direct effect of the mode on the flame motion can be delineated. This directly links the effect of mode II to the flame stabilization in the outer regions of the flame, as also observed from the instantaneous sequences.

Chapter 6
Summary of Publications

Paper I

J. Savre, H. Carlsson, X.S. Bai, "Turbulent methane/air premixed flame structure at high Karlovitz numbers". *Flow, Turbulence and Combustion* 90 (2013) 325-341.

In this paper 2D DNS was utilized to study the effect of the Karlovitz number on the flame structure in lean premixed methane/air flames. Flames with Karlovitz numbers ranging from 600 to 9500 were investigated and it was reported that the flames did not reach a distributed state for Karlovitz numbers below 2000. This observation was claimed to be due to the rapid dissipation of small scale turbulence as it penetrates the flame with corresponding viscosity increase. A modified Karlovitz number accounting for the density ratio of the observed flame was proposed, positioning solely the Ka = 9500 case in the distributed reaction zone regime during the entire simulation. Flame broadening as well as species concentration correlations with progress variable along with corresponding reaction rates was reported, presenting effect of distributed burning on the flame composition. Significant discrepancies from the flamelet profiles were observed.

The simulations were performed by Julien Savre. The candidate participated in analysis, post-processing, and writing of the paper along with the other authors.

Paper II

H. Carlsson, R. Yu, X.S. Bai, "Direct Numerical Simulation of Lean Premixed CH_4/Air and H_2/Air Flames at High Karlovitz Numbers". *International Journal of Hydrogen Energy*, in press (2014).

3D direct numerical simulations of turbulent premixed CH_4/air and H_2/air flames at high Karlovitz numbers were performed to study the influence of intense turbulence on the detailed chemistry structures of the flames. From a detailed analysis of the flame structures it was found that significant heat release rate was obtained at relatively low temperatures. Investigations of species reaction rates showed significant deviations from those of laminar

flames and flamelets. It was shown that the intensified heat release rate at low temperatures is a result of increased convection-diffusion transport of H radicals from the high temperature zones to the low temperature zones which magnified the reaction rates of exothermic low temperature reactions. The heat released from these reactions in laminar flames are typically negligible; however, in distributed flames it was shown that the heat release rate from these reactions could reach as high values as three times the peak heat release rate in a 1D flame. To further investigate the effects of diffusive transport on the observed phenomenon, 2D test simulations utilizing a unity Lewis number simplification of the diffusion coefficients showed that differential diffusion had a significant effect on the transport of H radicals from high to low temperatures and thereby the heat release rate at low temperatures.

The candidate performed the simulations and wrote the paper with feedback from the coauthors.

Paper III

H. Carlsson, R. Yu, X.S. Bai, "Flame Structure Analysis for Categorization of Lean Premixed CH_4/air and H_2/air Flames at High Karlovitz Numbers: Direct Numerical Simulation Studies". *Proceedings of the Combustion Institute*, in press (2014).

In turbulent premixed combustion at high Karlovitz numbers, interaction between intense small scale turbulence and different layers of the flame becomes important. In this paper, this kind of interactions in both H_2/air and CH_4/air flames were studied with direct numerical simulations. The two flames were studied at identical Karlovitz numbers (Ka = 1860); however, the layers of intermediate species within the two flames were affected significantly different by turbulence. Species specific Karlovitz numbers were defined and from these it was evident that the Karlovitz numbers based on the intermediate species H and HO_2 were significantly different between the two flames. By the use of Fourier transform analysis a turbulent effective chemical time scale was defined to determine the true effect of turbulence on the different reaction zone layers. Furthermore, through comparison between the turbulent effective chemical time scale and the laminar species specific time scale, validation of the species specific Karlovitz number could also be performed.

The candidate performed the simulations and wrote the paper with feedback from the coauthors.

Paper IV

A. Bohlin, E. Nordström, H. Carlsson, X.S. Bai, P.-E. Bengtsson, "Pure rotational CARS measurements of temperature and relative O_2-concentration in a low swirl turbulent premixed flame". *Proceedings of the Combustion Institute* 34 (2013) 3629-3636.

This paper presents pure rotational coherent anti-Stokes Raman (RCARS) spectroscopy in a turbulent premixed low swirl stabilized flame. Temperature as well as the relative concentration of O_2 were measured, where the accuracy of the temperature measurement has been proven less than 3% through extensive testing prior to this application of the technique. Measurements along the center axis of the burner was presented and compared to LES. Reasonable comparison between experiments and simulations was found. However, it was noted that the central lift-off was slightly under-predicted in LES and also that the air entrainment rate to burned gases was over-predicted. This new set of accurate mean and rms temperature data is of central importance for validation and development of boundary conditions as well as combustion model, since the measured range is covering the two most essential regions of the low swirl flame: the turbulent flame fluctuation as well as the air entrainment into burned gases.

Experiments were performed by Per-Erik Bengtsson, Alexis Bohlin, and Emil Nordström. Simulations were performed by the candidate, who also participated in analysis, post-processing and writing of the paper along with the coauthors.

Paper V

H. Carlsson, E. Nordström, A. Bohlin, P. Petersson, Y. Wu, R. Collin, M. Aldén, P.-E. Bengtsson, X.S. Bai, "Large Eddy Simulations and Rotational CARS/PIV/PLIF Measurements of a Lean Premixed Low Swirl Stabilized Flame". *Combustion and Flame* 161 (2014) 2539-2551.

This paper reports on an extensive validation campaign where LES were performed together with RCARS, particle image velocimetry (PIV), and planar laser induced fluorescence (PLIF) to study structures and statistical

quantities of a low swirl stabilized flame. The levelset G-equation combustion model for the LES was extended with a dynamic modeling approach for the subgrid scale flame wrinkling and evaluated for a Reynolds number higher than that previously studied with the model. The validation revealed that the flame could be considered well captured with the present flamelet model and that the dynamic implementation of the subgrid scale flame wrinkling showed an overall better agreement with the experimental data than the non-dynamic model did. The simulations were able to capture both the turbulent fluctuation of the leading edge of the flame as well as the cooling of the combustion products by entrainment of the ambient air. These have been, and still pose, severe difficulties for combustion models and fluid simulations applied to low swirl flames.

Large eddy simulations were performed by the candidate. Rotational CARS measurements were performed by Per-Erik Bengtsson, Alexis Bohlin, and Emil Nordström. PIV and PLIF measurements were performed by Per Petersson and Robert Collin. The candidate was managing the assembly of the paper and contributed to a major part of analysis, post-processing of data, and writing of the paper with feedbacks from the coauthors.

Paper VI

H. Carlsson, C. Carlsson, L. Fuchs, X.S. Bai, "Large Eddy Simulation and Extended Dynamic Mode Decomposition of Flow-Flame Interaction in a Lean Premixed Low Swirl Stabilized Flame". *Flow, Turbulence and Combustion* 93 (2014) 505-519.

In this paper we presented large eddy simulations and analysis of the flame dynamics in a low swirl burner. Distinct frequencies were found in Fourier transforms of velocity data in the different shear layer regions of the flow field. By performing an extended version of dynamic mode decomposition (EDMD), modes of combined flow and flame variables could be extracted. By the use of this method the different effects on the flame motion from the two dominating frequencies in the flow field (with origin in the inner and outer shear layers of the burner flow field, respectively) could be scrutinized. It was shown that the coherent structures linked to the inner shear layer frequency had a significant effect on the flame motion whereas the coherent structures with origin in the outer shear layer had no discernible effect on the flame. The inner shear layer generated mode was further analyzed and the net effect on the flame was linked to the inner shear

layer generated vorticity which was stated as a contributing factor to the flame stabilization mechanism in previous work [78].

The candidate performed the simulations and carried out the analysis together with Christian Carlsson. The paper was written by the candidate and Christian Carlsson with feedback from the coauthors.

Chapter 7
Concluding Remarks and Future Work

7.1. Concluding Remarks

In this thesis flame/turbulence interaction at moderate and high Karlovitz numbers has been investigated using direct numerical simulation and large eddy simulation. The direct numerical simulation (DNS) has been primarily focused on premixed flames in the distributed reaction zone regime whereas the large eddy simulation (LES) has been utilized for studies of swirl stabilized flames in the flamelet and thin-reaction zone regimes.

The DNS of high Karlovitz number flames showed that the intensified transport of heat, radicals, and major species within the premixed flame structure effectively broadens the preheat zone and the reaction zone of the flame. In particular, the redistribution of radicals is shown to significantly affect the reaction rates of various species and reaction rates in the low temperature zone. This effect is typically negligible in low Karlovitz number flames, but it is drastically magnified and becomes non-negligible at high Karlovitz numbers. Special focus has been put to investigate the redistribution of H radicals, which, as it enters the low temperature zone, significantly magnifies the reaction rate of an exothermic three-body recombination reaction ($H+O_2+M \rightarrow HO_2+M$). It has been shown that the amplification of this reaction locally raises the heat release rate and that a significant heat release rate in the low temperature range can be obtained in high Karlovitz number flames.

During the studies of high Karlovitz number flames, significant differences between a CH_4/air and an H_2/air flame with identical Karlovitz numbers in terms of the turbulence effect on different radical layers were noted. Since the conventional Karlovitz number and Damköhler number categorization of these flames was unable to describe these differences, a new species-specific Karlovitz number was proposed. Validation studies confirmed that this non-dimensional number was able to account for the difference between the two flames and also for the difference in turbulence interaction with different radical layers.

LES with the G-equation combustion model for stratified premixed flames has been successfully employed for swirl stabilized premixed flames in the thin-reaction zone combustion regime. The wrinkling factor sub-

model for the G-equation model employed for LES has been made dynamic and using this model, velocity and scalar measurements have been reproduced with reasonable agreement for varying operating conditions.

The LES results are also used for flow-flame interaction studies where an extended version of dynamic mode decomposition (EDMD) was employed for the combined set of velocity variables and a flame marking variable (the G-field) to extract which coherent frequency specific modes in the flow field that had a significant effect on the flame motion. The EDMD analysis was able to distinguish the effect of the inner shear layer generated vorticity from the outer shear layer generated one on the flame motion, which therefore can be a useful tool for analysis of frequency specific coherent structures during combustor design stages.

7.2. Future Work

The novel studies of high Karlovitz number flames performed in this thesis have both found and opened new doors towards follow-up studies. High Karlovitz number flames will be of more pronounced industrial relevance in the future and it is therefore important to obtain a comprehensive understanding of such flames as soon as possible. To continue this work the following topics are of high relevance:

- Performing extended analysis of the non-linear coupled system of elementary reaction rates to further quantify the influence of individual elementary reactions
- Conduct parameter studies on the effect of Karlovitz number on the in-flame turbulent transport and detailed chemistry
- Study the effect of high Karlovitz number combustion for different fuels, e.g., longer hydrocarbons

There are also several things that can be done to continue the work on large eddy simulation combustion modeling of swirl stabilized lean premixed flames and studies of flow-flame interaction in such flames, e.g.,

- Study the influence of confinement, elevated pressure, and compressibility effects on the modeling of premixed flames
- Incorporate the mechanisms of radiation heat loss and the effect of re-burning of fuel that “leaks” through quenched parts of the flame and study their effect on the flame

- The mode decomposition analysis should also be performed for experimental data in order to validate/disproof the prediction from LES

Finally, the two different approaches in this thesis should be combined by utilizing the DNS database to develop refined subgrid scale models for turbulent premixed flames at moderate and high Karlovitz numbers.

Bibliography

[1] F.A. Williams, *Combustion Theory*, 2nd edition, The Benjamin/Cummings Publishing Company, Inc. California 1985.

[2] M.S. Mansour, N. Peters, Y.C. Chen, Investigation of scalar mixing in the thin reaction zones regime using a simultaneous CH LIF/Rayleigh laser technique, *Proc. Combust. Inst.* 27 (1998) 767-773.

[3] Z.S. Li J. Kiefer, J. Zetterberg, M. Linvin, A. Leipertz, X.S. Bai, M. Aldén, Development of improved PLIF CH detection using an Alexandrite laser for single-shot investigation of turbulent and lean flames, *Proc. Combust. Inst.* 31 (2007) 727-735.

[4] J. Kiefer, Z.S. Li, J. Zetterberg, X.S. Bai, M. Aldén, Investigation of local flame structures and statistics in partially premixed turbulent jet flames using simultaneous single-shot CH and OH planar laser-induced fluorescence imaging, *Combust. Flame* 154 (2008) 802-818.

[5] Z.S. Li, B. Li, Z.W. Sun, X.S. Bai, M. Aldén, Turbulence and combustion interaction: High resolution local flame front structure visualization using simultaneous single-shot PLIF imaging of CH, OH and CH2O in a piloted premixed jet flame, *Combust. Flame* 157 (2010) 1087-1096.

[6] J. Sjöholm, J. Rosell, B. Li, M. Richter, Z.S. Li, X.S. Bai, M. Aldén, Simultaneous measurements of OH, CH, CH2O and Toluene LIF in a methane jet flame with varying degrees of turbulence, *Proc. Combust. Inst*. 34 (2013) 1475-1482.

[7] B. Zhou, C. Brackmann, Z.S. Li, M. Aldén, X.S. Bai, Simultaneous multi-species and temperature visualization of premixed flames in the distributed reaction zone regime, *Proc. Combust. Inst.* (2014) http://dx.doi.org/10.1016/j.proci.2014.06.107.

[8] B. Bedat, R.K. Cheng, Experimental study of premixed flames in intense isotropic turbulence, *Combust. Flame* 100 (1995) 285-294.

[9] O. Reynolds, On the dynamical theory of incompressible viscous flows and the determination of the criterion, *Philos. Trans. R. Soc. London Ser. A* 186 (1894) 123-161.

[10] L.F. Richardson, *Weather prediction by numerical process*, Cambridge University Press 1922.

[11] S.B. Pope, *Turbulent Flows*, Cambridge University press, 2009.

[12] A.N. Kolmogorov, The local structure of turbulence in incompressible viscous fluid for very large Reynolds numbers (orig. in Russian), *Dokl. Akad. Nauk SSSR* 30 (1941) 299-303.
[13] M.D. Smooke, V. Giovangigli, *Formation of the premixed and nonpremixed test problems*, in: Reduced kinetic mechanisms and asymptotic approximation for methane-air flames, Springer Verlag, Berlin, 1991.
[14] K. Seshadri, N. Peters, The inner structure of methane-air flames, *Combust. Flame* 81 (1990) 96-118.
[15] R. Borghi, Turbulent combustion modeling, *Prog. Energy Combust. Sci.* 14 (1988) 245-292.
[16] N. Peters, *Turbulent combustion*, Cambridge: Cambridge University Press 2000.
[17] N. Swaminathan, K.N.C. Bray, Turbulent premixed flames, Cambridge University Press 2011.
[18] Y.C. Chen, N. Peters, G.A. Schneemann, N. Wruck, U. Renz, M.S. Mansour, The detailed flame structure of highly stretched turbulent premixed methane-air flames, *Combust. Flame* 107 (1996) 223-244.
[19] A.M. Steinberg, J.F. Driscoll, Straining and wrinkling processes during turbulence – premixed flame interaction measured using temporally resolved diagnostics, *Combust. Flame* 156 (2009) 2285-2306.
[20] A.M. Steinberg, J.F. Driscoll, Stretch-rate relationships for turbulent premixed combustion LES subgrid models measured using temporally resolved diagnostics, *Combust. Flame* 157 (2010) 1422-1435.
[21] T. Poinsot, D. Veynante, *Theoretical and Numerical Combustion*, Edwards 2001.
[22] H. Pitsch, L. Duchamp de Lageneste, Large-eddy simulation of premixed turbulent combustion using a level-set approach, *Proc. Combust. Inst.* 29 (2002) 2001-2008.
[23] H. Pitsch, Large-Eddy Simulation of Turbulent Combustion, *Ann. Rev. Fluid Mech.* 28 (2006) 453-482.
[24] J.F. Driscoll, Turbulent premixed combustion: Flamelet structure and its effect on turbulent burning velocities, *Prog. Ener. Combust. Sci.* 34 (2008) 91-134.
[25] L.P.H. de Goey, T. Plessing, R.T.E. Hermanns, N. Peters, Analysis of the flame thickness of turbulent flamelets in the thin reaction zones regime, *Proc. Combust. Inst.* 30 (2005) 859-866.

[26] Y.C. Chen, M.S. Mansour, Investigation of flame broadening in turbulent premixed flames in the thin-reaction-zones regime, *Symp. (Int.) Combust.* 27 (1998) 811-818.
[27] R. Sankaran, E.R. Hawkes, J.H. Chen, T. Lu, C.K. Law, Structure of a spatially developing turbulent lean methane-air Bunsen flame, *Proc. Combust. Inst.* 31 (2007) 1291-1298.
[28] A.Y. Poludnenko, E.S. Oran, The interaction of high-speed turbulence with flames: global properties and internal flame structure, *Combust. Flame.* 157 (2010) 995-1011.
[29] M.J. Dunn, A.R. Masri, R.W. Bilger, A new piloted premixed jet burner to study strong finite-rate chemistry effects, *Combust. Flame* 151 (2007) 46-60.
[30] U. Stopper, W. Meier, R. Sadanandan, M. Stöhr, M. Aigner, G. Bulat, Experimental study of industrial gas turbine flames including quantification of pressure influence on flow field, fuel/air premixing and flame shape, *Combust. Flame* 160 (2013) 2103-2118.
[31] P. Strakey, T. Sidwell, J. Ontko, Investigation of the effects of hydrogen addition on lean extinction in a swirl stabilized combustor, *Proc. Combust. Inst.* 31 (2007) 3173-3180.
[32] J.B. Bell, R.K. Cheng, M.S. Day, I.G. Shepherd, Numerical simulation of Lewis number effects on lean premixed turbulent flames, *Proc. Combust. Inst.* 31 (2007) 1309-1317.
[33] M. Day, J. Bell, P.T. Bremer, V. Pascucci, V. Beckner, M. Lijewski, Turbulence effects on cellular burning structures in lean premixed hydrogen flames, *Combust. Flame* 156 (2009) 1035-1045.
[34] C.J. Pope R.A. Shandross, J.B. Howard, Variation of equivalence ratio and element ratios with distance from burner in premixed one-dimensional flames, *Combust. Flame* 116 (1999) 605-614.
[35] A.J. Aspden, J.B. Bell, S.E. Woosley, Distributed Flames in Type Ia Supernovae, *Astrophysical J.* 710 (2010) 1654-1663.
[36] A.J. Aspden, M.S. Day, J.B. Bell, Turbulence-flame interactions in lean premixed hydrogen: transition to the distributed burning regime, *J. Fluid Mech.* 680 (2011) 287-320.
[37] A.J. Aspden, M.S. Day, J.B. Bell, Characterization of low Lewis number flames, *Proc. Combust. Inst.* 33 (2011) 1463-1471.
[38] A.J. Aspden, M.S. Day, J.B. Bell, Lewis number effects in distributed flames, *Proc. Combust. Inst.* 33 (2011) 1473-1480.

[39] R. Yu, J. Yu, X.S. Bai, An improved high-order scheme for DNS of low Mach number turbulent reacting flows based on stiff chemistry solver, *J. Comp. Phys.* 231 (2012) 5504-5521.

[40] N. Chakraborty, R.S. Cant, Influence of Lewis number on strain rate effects in turbulent premixed flame propagation, *Int. J. Heat Mass Transfer* 46 (2006) 2158-2172.

[41] R. Sankaran, E.R. Hawkes, J.H. Chen, T. Lu, C.H. Law, Structure of a spatially developing turbulent lean methane–air Bunsen flame, *Proc. Combust. Inst.* 31 (2007) 1291-1298.

[42] J.H. Chen, Petascale direct numerical simulation of turbulent combustion-fundamental insights towards predictive models, *Proc. Combust. Inst.* 33 (2011) 99-123.

[43] A.N. Kolmogorov, Dissipation of energy in locally isotropic turbulence, *Dokl. Akad. Nauk SSSR* 32 (1941) 19-21.

[44] J. Smagorinsky, General circulation experiments with the primitive equations: I. the basic equations, *Mon. Weather Rev.* 91 (1963) 81-164.

[45] A.N. Kolmogorov, The equations of turbulent motion in an incompressible fluid (orig. in Russian), *Izvestia Akad. Sci., USSR; Phys*. 6 (1942) 56-58.

[46] L. Prandtl, Über ein neues Formelsystem für die ausgebildete Turbulenz, *Nachr. Akad. Wiss. Göttingen Math-Phys. K1* (1945) 6-19.

[47] J. Bardina, J.H. Ferziger, W.C. Reynolds, Improved subgrid-scale models for large-eddy simulation, *AIAA paper No.* (1980) 80-1357.

[48] A. Germano, U. Piomelli, P. Moin, W.H. Cabot, A dynamic subgrid-scale eddy viscosity model, *Phys. Fluids* 3 (1991) 1760-1765.

[49] J.C. Tannehill, D.A. Anderson, R.H. Pletcher, *Computational Fluid Mechanics and Heat Transfer*, 2nd edition, Taylor and Francis 1997.

[50] C. Fureby, F.F. Grinstein, Large Eddy Simulation of High-Reynolds-Number Free and Wall-Bounded Flows, *J. Comp. Phys.* 181 (2002) 68-97.

[51] F.F. Grinstein, L.G. Margolin, W.J. Rider (Eds.), *Implicit Large Eddy Simulation, computing turbulent Fluid Dynamics*, Cambridge University Press, UK, 2007.

[52] J. Li, Z. Zhao, A. Kazakov, F.L. Dryer, An Updated Comprehensive Kinetic Model of Hydrogen Combustion, *Int. J. Chem. Kinet.* 36 (2004) 566-575.

[53] K.J. Nogenmyr, C. Fureby, X.S. Bai, P. Petersson, R. Collin, M. Linne, Large eddy simulation and laser diagnostic studies on a low swirl stratified premixed flame, *Combust. Flame* 156 (2009) 25-36.

[54] P. Nilsson, X.S. Bai, Effects of flame stretch and wrinkling on co formation in turbulent premixed combustion, *Proc. Combust. Inst.* 29 (2002) 1873-1879.

[55] P. Wang, X.S. Bai, Large eddy simulation of turbulent premixed flames using level-set G-equation, *Proc. Combust. Inst.* 30 (2005) 583-591.

[56] M. Dusing, A. Kempf, F. Flemming, A. Sadiki, J. Janicka, Combustion LES for Premixed and Diffusion Flames, *Prog. Comput. Fluid Dyn*. 5 (2005) 363-374.

[57] G.S. Strang, On the Construction and Comparison of Difference Schemes, SIAM J. Num. Anal. 5 (1968) 506-517.

[58] S. Gottlieb, C.W. Shu, Total variation diminishing Runge-Kutta schemes, *Math. Comp.* 67 (1998) 73–85.

[59] G.S. Jiang, D.P. Peng, Weighted ENO schemes for Hamilton-Jacobi equations, *SIAM J. Sci. Comp.* 21 (2000) 2126–2143.

[60] P.N. Brown, G.D. Byrne, A.C. Hindmarsh, VODE –A Variable-coefficient ODE solver, *Siam J. Sci. Stat. Comp*. 10 (1989) 1038-1051.

[61] R. Yu, *Large Eddy Simulation of Turbulent Flow and Combustion in HCCI engines*, Lund University, 2008.

[62] R. Yu, X.S. Bai, A semi-implicit scheme for large eddy simulation of piston engine and combustion, *Int. J. Numer. Meth. Fluids* 71 (2013) 13-40.

[63] http://code.google.com/p/pencil-code/, (2011).

[64] N. Babkovskaia, N.E.L. Haugen, A. Brandenburg, A high-order public domain code for direct numerical simulations of turbulent combustion, *J. Comp. Phys.* 230 (2011) 1-12.

[65] J.O. Hinze, *Turbulence*, 2nd edition, McGraw-Hill, 1975.

[66] R.H. Kraichnan, Diffusion by a random velocity field, *Phys. Fluids* 13 (1970) 22-31.

[67] A. Careta, F. Sagues, J.M. Sancho, Generation of homogeneous isotropic turbulence with well-defined spectra, *Phy. Rev. E*. 48 (1993) 2279-2287.

[68] R. Yu, X.S. Bai, A fully divergence-free method for generation of inhomogeneous and anisotropic turbulence with large spatial variation, *J. Comput. Phys.* 256 (2014) 234-253.

[69] C.J. Rutland, A. Trouvé, Direct simulations of premixed turbulent flames with nonunity Lewis numbers, *Combust. Flame* 94 (1993) 41-57.

[70] S.B. Pope, P.K. Yeung, S.S. Girimaji, The curvature of material surfaces in isotropic turbulence, *Phys. Fluids* A 1 (1989) 2010-2018.

[71] T. Poinsot, S. Candel, A. Trouvé, Applications of Direct Numerical Simulation to premixed turbulent combustion, *Prog. Energy Combust. Sci.* 21 (1996) 531-576.

[72] J. Gullbrand, X.S. Bai, L. Fuchs, High order Cartesian grid method for calculation of incompressible turbulent flows, *Int. J. Numer. Meth. Fluids* 36 (2001) 687-709.

[73] M.M. Rai, P. Moin, Direct simulations of turbulent flow using finite-difference schemes, *J. Comp. Phys*. 96 (1991) 15–53.

[74] C.W. Rowley, I. Mezic, S. Baheri, P. Schlatter, D.S. Henningson, Spectral analysis of nonlinear flows, *J. Fluid Mech.* 641 (2009) 115-127.

[75] P.J. Schmid, Dynamic mode decomposition of numerical and experimental data, *J. Fluid Mech.* 656 (2010) 5-28.

[76] P. Petersson, J. Olofsson, C. Brackman, H. Seyfried, J. Zetterberg, M. Richter, M. Aldén, M.A. Linne, R.K. Cheng, A. Nauert, D. Geyer, A. Dreizler, Simultaneous PIV/OH-PLIF, Rayleigh thermometry/OH-PLIF and stereo PIV measurements in a low-swirl flame, *Appl. Opt.* 46 (2007) 3928-3936.

[77] K.J. Nogenmyr, P. Petersson, X.S. Bai, A. Nauert, J. Olofsson, C. Brackman, H. Seyfried, J. Zetterberg, Z.S. Li, M. Richter, A. Dreizler, M. Linne, M. Aldén, Large eddy simulation and experiments of stratified lean premixed methane/air turbulent flames, *Proc. Combust. Inst.* 31 (2007) 1467-1475.

[78] K.J. Nogenmyr, P. Petersson, X.S. Bai, C. Fureby, R. Collin, A. Lantz, M. Linne, M. Aldén, Structure and stabilization mechanism of a stratified premixed low swirl flame, *Proc. Combust. Inst*. 33 (2011) 1567-1574.

[79] M. Day, S. Tachibana, J. Bell, M. Lijewsi, V. Beckner, R.K. Cheng, A combined computational and experimental characterization of lean premixed turbulent low swirl laboratory flames: I. Methane flames, *Combust. Flame* 159 (2012) 275-290.

[80] P. Petersson, R. Wellander, J. Olofsson, H. Carlsson, C. Carlsson, B.B. Watz, N. Boetkjaer, M. Richter, M. Aldén, L. Fuchs, X.S. Bai, Simultaneous High-Speed PIV and OH PLIF Measurements and

Modal Analysis for Investigating Flame-Flow Interaction in a Low Swirl Flame, *16th International Symposium on Applications of Laser Techniques to Fluid Mechanics*, Lisbon, Portugal (2012).

[81] H. Carlsson, P. Petersson, C. Carlsson, R. Wellander, M. Richter, L. Fuchs, X.S. Bai, M. Aldén, Flame Speed Analysis in a Methane/Air Low Swirl Premixed Flame, *6th European Combustion Meeting Paper P4-63*, Lund, Sweden (2013).

[82] R.K Cheng, Velocity and scalar characteristics of premixed turbulent flames stabilized by weak swirl, *Combust. Flame* 101 (1995) 1-14.

[83] R.K. Cheng, I.G. Shepherd, B. Bedat, L. Talbot, Premixed turbulent flame structures in moderate and intense isotropic turbulence, *Combust. Sci. Tech.* 174 (2002) 29-59.

[84] I.G. Shepherd, R.K. Cheng, T. Plessing, C. Kortschik, N. Peters, Premixed flame front structure in intense turbulence, *Proc. Combust. Inst.* 29 (2002) 1833-1840.

[85] M. Mansour, Y.C. Chen, Stability characteristics and flame structure of low swirl burner, *Exp. Therm. Fluid Sci.* 32 (2008) 1390-1395.